



# A multi-isotope study (Fe, Ge, O) of hydrothermal alteration in the Limousin ophiolite (French Massif Central)

Afifé El Korh, Marie-Christine Boiron, Damien Cividini

## ► To cite this version:

Afifé El Korh, Marie-Christine Boiron, Damien Cividini. A multi-isotope study (Fe, Ge, O) of hydrothermal alteration in the Limousin ophiolite (French Massif Central). *Lithos*, 2020, 378-379, pp.105876. 10.1016/j.lithos.2020.105876 . hal-03135104

**HAL Id: hal-03135104**

**<https://hal.univ-lorraine.fr/hal-03135104>**

Submitted on 9 Feb 2021

**HAL** is a multi-disciplinary open access archive for the deposit and dissemination of scientific research documents, whether they are published or not. The documents may come from teaching and research institutions in France or abroad, or from public or private research centers.

L'archive ouverte pluridisciplinaire **HAL**, est destinée au dépôt et à la diffusion de documents scientifiques de niveau recherche, publiés ou non, émanant des établissements d'enseignement et de recherche français ou étrangers, des laboratoires publics ou privés.



Distributed under a Creative Commons Attribution 4.0 International License



## Research Article

# A multi-isotope study (Fe, Ge, O) of hydrothermal alteration in the Limousin ophiolite (French Massif Central)

Affé El Korh<sup>a,\*</sup>, Marie-Christine Boiron<sup>b</sup>, Damien Cividini<sup>c</sup>

<sup>a</sup> Unit of Earth Sciences, Department of Geosciences, University of Fribourg, Chemin du Musée 6, CH-1700 Fribourg, Switzerland

<sup>b</sup> Université de Lorraine, CNRS, GeoResources, F-54000 Nancy, France

<sup>c</sup> Centre de Recherches Pétrographiques et Géochimiques (CRPG), UMR 7358 CNRS-Université de Lorraine, 15 rue Notre Dame des Pauvres, BP 20, F-54501 Vandœuvre-lès-Nancy Cedex, France



## ARTICLE INFO

## Article history:

Received 9 August 2020

Received in revised form 17 October 2020

Accepted 9 November 2020

Available online 12 November 2020

## Keywords:

Iron isotopes

Germanium isotopes

Oxygen isotopes

Serpentinities

Amphibolites

Ophiolite

## ABSTRACT

Geochemical studies using non-traditional stable isotopes can help tracing processes of hydrothermal alteration (or hydrothermal metamorphism) of ancient oceanic lithosphere. In this study, we have measured non-traditional Ge and Fe isotopes and traditional O isotopes in a series of ultrabasic and basic rocks from the Limousin ophiolite (French Massif Central) to decipher the different signatures of hydrothermal vs. magmatic processes. Serpentinities are strongly oxidised rocks ( $\text{Fe}^{3+}/\Sigma\text{Fe}$ : 0.58–0.71) and display  $\delta^{18}\text{O}$  values (+5.0 to +6.1‰) typical of hydrothermally altered ultrabasic rocks. They display  $\delta^{56}\text{Fe}$  (+0.15 to +0.18‰) and  $\delta^{74}\text{Ge}$  values (+0.48 to +0.93‰) similar to heavier than ultrabasic rocks. The negative correlation between  $\delta^{18}\text{O}$  and  $\delta^{74}\text{Ge}$  and between  $\delta^{18}\text{O}$  and  $\delta^{56}\text{Fe}$ , suggests that Ge and Fe isotopes have fractionated during hydrothermal alteration. The  $\delta^{74}\text{Ge}$  shows a slight positive correlation with the  $\delta^{56}\text{Fe}$ , indicating concomitant Ge and Fe isotope fractionation towards heavier values during hydrothermal alteration. However,  $\delta^{56}\text{Fe}$  values display a larger deviation from ultrabasic rocks than  $\delta^{74}\text{Ge}$  and  $\delta^{18}\text{O}$  values, suggesting that oxidising conditions have enhanced Fe isotope fractionation to a larger extent than Ge isotopes. Amphibolites display  $\text{Fe}^{3+}/\Sigma\text{Fe}$  ratios (0.11–0.14) and  $\delta^{56}\text{Fe}$  values (+0.03 to +0.17‰) typical of mid-ocean ridge basalts (MORB).  $\delta^{18}\text{O}$  values are typical of high-T hydrothermally altered MORB (+6.2 to +6.6‰).  $\delta^{74}\text{Ge}$  values show a small range (+0.72 to +0.77‰) and are heavier than most basalts and gabbros. The  $\delta^{18}\text{O}$  slightly decreases with the increase of the  $\delta^{56}\text{Fe}$ , indicating that Fe isotopes may have fractionated towards lighter values during hydrothermal alteration. However, the lack of correlation between  $\delta^{74}\text{Ge}$  and  $\delta^{56}\text{Fe}$  values indicates that Ge isotope fractionation has prevailed over Fe isotope fractionation during hydrothermal alteration of basic rocks in the absence of oxidising conditions.

© 2020 The Author(s). Published by Elsevier B.V. This is an open access article under the CC BY license (<http://creativecommons.org/licenses/by/4.0/>).

## 1. Introduction

Ophiolite-derived rocks composed of ultrabasic (peridotites, serpentinites) and basic rocks (gabbros, basalts) are remnants of ancient oceanic lithosphere that were accreted in convergent settings by subduction/exhumation or obduction processes. Fluid-rock interactions in subducted plates and ophiolites may be sources of significant mass transfer between the oceanic lithosphere and the fluid and volatile phases. The oceanic lithosphere undergoes various stages of hydrothermal alteration (or hydrothermal metamorphism) from its formation along mid-oceanic ridge to its accretion in convergent settings (e.g. Beinlich et al., 2010; Cartwright and Barnicoat, 1999; Muehlenbachs, 1998): 1) High-temperature (high-T;  $T > 350^\circ\text{C}$  up to late magmatic conditions) hydrothermally alteration close to spreading ridges and black smokers is responsible for Ca enrichment and Mg depletion in basic rocks, as well as for a decrease of the  $\delta^{18}\text{O}$  compared to mid-

ocean ridge basalts (MORB;  $\delta^{18}\text{O} = +5.8 \pm 0.3\%$ ; Muehlenbachs, 1998, and references therein). Sulphides may precipitate on the ocean floor in black-smoker-type deposits, while gabbros are altered into epidiosites under black-smokers; 2) Low-temperature (low-T;  $T$  from  $<100^\circ\text{C}$  to  $350^\circ\text{C}$ ) alteration in the upper part of the oceanic lithosphere is responsible for Mg enrichment, Ca depletion, and for a  $\delta^{18}\text{O}$  increase compared to MORB. The  $\delta^{18}\text{O}$  decreases with depth, i.e. with decreasing the amount of percolating fluids in the deeper parts of the ocean crust (gabbros); 3) Fluid-rock interactions during devolatilisation reactions related to subduction zone metamorphism if the oceanic lithosphere is subducted; 4) Fluid-rock interactions related to low- to medium-pressure metamorphism during obduction/exhumation of ophiolites related to orogenic processes; and 5) Migration of late- to post-orogenic fluids.

Studies on stable Fe and Ge isotopes showed that they can fractionate at both low-T and high-T magmatic and hydrothermal conditions and can be employed as tracers of magmatic, metamorphic and hydrothermal processes (for a review, see Sossi et al., 2016; El Korh et al., 2017a; Rouxel and Luais, 2017; Johnson et al., 2020).

\* Corresponding author.

E-mail address: [afife.elkorh@unifr.ch](mailto:afife.elkorh@unifr.ch) (A. El Korh).

Iron isotopes (masses 54, 56, 57 and 58) can fractionate among Earth reservoirs, especially if changes in redox conditions and bonding environment are involved (e.g. Polyakov and Mineev, 2000; Sossi and O'Neill, 2017). Deviation of the  $^x\text{Fe}/^{54}\text{Fe}$  ratio is expressed as  $\delta^x\text{Fe} = [(^x\text{Fe}/^{54}\text{Fe})_{\text{sample}} / (^x\text{Fe}/^{54}\text{Fe})_{\text{IRMM-014}} - 1] \times 1000$  (with  $x = 56$  or 57), relative to the IRMM-014 Fe standard solution. Fe isotope fractionation in magmatic rocks mainly results from: 1) partial melting (Teng et al., 2013; Weyer and Ionov, 2007; Williams et al., 2005); 2) fractional crystallisation (Sossi et al., 2012); 3) variations in mantle oxidation state and oxygen fugacity (Dauphas et al., 2009; Williams et al., 2005) and; 4) mantle metasomatism resulting from subduction of isotopically variable oceanic crust and Fe transport through fluid migration in the deep mantle (Beard and Johnson, 2004; Poitrasson et al., 2013; Zhao et al., 2010). Magmatic and metasomatic processes are responsible for the heavier Fe isotopic signatures of oceanic basalts [MORB, ocean island basalts (OIB), and back arc basin basalts (BABB)] compared to the bulk Earth mantle [ $+0.034 \pm 0.01\%$ ;  $2\sigma$  standard error (SE)], mantle rocks (Cr-rich dunites, peridotites and xenoliths:  $\delta^{56}\text{Fe}$  from  $-0.540$  to  $+0.173\%$ ) and island arc basalts ( $\delta^{56}\text{Fe}$  from  $-0.037$  to  $+0.143\%$ ) (Craddock et al., 2013; Dauphas et al., 2009; Konter et al., 2016; Nebel et al., 2013, 2015; Poitrasson et al., 2013; Sossi et al., 2016; Su et al., 2015; Weyer and Ionov, 2007; Zhang et al., 2019, 2020; Zhao et al., 2010, 2017). Besides, Fe isotopic compositions of MORB and BABB ( $\delta^{56}\text{Fe}$  from  $+0.026$  to  $+0.176\%$ ) cover a smaller range than OIB ( $\delta^{56}\text{Fe}$  from  $-0.011$  to  $+0.300\%$ ) (Konter et al., 2016; Nebel et al., 2013; Schuessler et al., 2009; Sossi et al., 2016; Teng et al., 2008, 2013; Weyer and Ionov, 2007).

During hydrothermal metamorphism of the oceanic lithosphere, significant changes in redox conditions are associated with dissolution and precipitation of Fe-bearing minerals on (sub-)seafloor. Because of the higher solubility of  $\text{Fe}^{2+}$  compared to  $\text{Fe}^{3+}$  in hydrous fluids, hydrothermal processes under reducing conditions produce fluids enriched in light-Fe isotopes, as well as high-T basalt-hosted vent fluids from mid-ocean ridges with a  $\delta^{56}\text{Fe}$  lower of c.  $-0.2$  to  $-0.7\%$  than igneous rocks (Bennett et al., 2009; Rouxel et al., 2008). Fe is mainly transported as Fe-chloride complexes in fluids (Manning, 2004). Changes in the non-redox parameters [such as ligand composition (chloride, sulphide), speciation, Fe coordination] is also expected to trigger Fe isotope fractionation in Fe-bearing solutions (Hill et al., 2010).

Hydrothermal alteration produces  $\text{Fe}^{2+}$ -bearing phases (e.g. Fe-sulphides) that are generally isotopically lighter than  $\text{Fe}^{3+}$ -bearing secondary products (e.g. Fe-rich clays or Fe-hydroxides), which show higher  $\delta^{56}\text{Fe}$  values than fresh MORB (Bennett et al., 2009; Polyakov and Mineev, 2000; Rouxel et al., 2003). The variety of alteration products results in highly heterogeneous Fe isotopic compositions of the altered oceanic crust, although similar in mean to the MORB value ( $\delta^{56}\text{Fe}$  from  $-0.73$  to  $+1.39\%$ ; mean:  $+0.08 \pm 0.13\%$ ;  $2\sigma$  SE; Rouxel et al., 2003; Williams et al., 2009). Besides, hydrothermal alteration of abyssal peridotites produces abyssal serpentinites with high  $\text{Fe}^{3+}/\Sigma\text{Fe}$  ratios (Debret et al., 2014; Mével, 2003) and  $\delta^{56}\text{Fe}$  ranging from  $-0.10\%$  to  $+0.11\%$  (Craddock et al., 2013; Debret et al., 2016).

Germanium is a trace element in most silicate rocks. Because of its oxidation state of 4+ and similar ionic and covalent radii to Si, Ge can be incorporated into  $\text{SiO}_2$  tetrahedras (Bernstein, 1985). Its five naturally occurring stable isotopes (masses 70, 72, 73, 74 and 76) can fractionate, with  $\delta^x\text{Ge} = [(^x\text{Ge}/^{70}\text{Ge})_{\text{sample}} / (^x\text{Ge}/^{70}\text{Ge})_{\text{NIST3120a}} - 1] \times 1000$  (with  $x = 72, 73$  or 74), relative to the NIST 3120a Ge standard solution. Ge isotope fractionation is relatively restricted at high-T magmatic conditions ( $T > 800^\circ\text{C}$ ), with  $\delta^{74}\text{Ge}$  ranging from  $+0.37$  to  $+0.68\%$  in ultrabasic, basic and granitic rocks (Escoubé et al., 2012, 2015; Luais, 2012; Rouxel et al., 2006; Rouxel and Luais, 2017).

Germanium speciation in fluids is relatively similar to that of aqueous Si (Wood and Samson, 2006). Because of the lower enthalpy and heat capacity of  $\text{Si}(\text{OH})_4(\text{aq})$  species compared to  $\text{Ge}(\text{OH})_4(\text{aq})$  species, the Ge/Si ratio of fluids in equilibrium with Ge-rich silicates increases

with temperature (Pokrovski and Schott, 1998). Ge shares a strong affinity with Fe hydroxides and can co-precipitate with Fe during  $\text{Fe}^{2+}$  oxidation or  $\text{Fe}^{3+}$  hydrolysis (Pokrovsky et al., 2014). Thus, Ge behaviour varies according to the physico-chemical conditions of hydrothermal alteration of the basaltic crust: 1) Ge depletion during high-T alteration along hydrothermal vents if hydrothermal sulphides precipitate or; 2) Ge enrichment due to Ge adsorption by iron hydroxides (Escoubé et al., 2015; Pokrovsky et al., 2014).

Ge isotope fractionation is strongly sensitive to the nature of precipitated minerals and alteration products during low-T hydrothermal alteration, yielding large  $\delta^{74}\text{Ge}$  variations in marine hydrothermal Fe-rich deposits ( $-0.98$  to  $+0.16\%$ ) and sulphide deposits ( $-4.71$  to  $-2.98\%$ ) (Escoubé et al., 2012, 2015; Rouxel et al., 2006). Hydrothermal vent fluids have heavy-Ge isotopic compositions ( $+0.61$  to  $+2.20\%$ ), which remain lower than the estimated  $\delta^{74}\text{Ge}$  value of seawater ( $+3.00\%$ ) (Escoubé et al., 2015). Quantification of equilibrium Ge isotope fractionation between fluids and minerals predicts that heavier Ge isotopes are enriched in minerals with shorter Ge–O bond lengths (Li et al., 2009). Thus, fluids in equilibrium with olivine are expected to be isotopically heavier than the solid phase (Rouxel and Luais, 2017), resulting in higher  $\delta^{74}\text{Ge}$  measured in serpentinites compared to unaltered ultrabasic rocks (Luais, 2012).

Recent studies have shown that the subducted oceanic crust can conserve the Fe and Ge isotopic composition of their hydrothermally altered basic protolith during high-pressure (HP) metamorphism (Beard and Johnson, 2004; Li et al., 2016; El Korh et al., 2017a, 2017b; Inglis et al., 2017), while Fe isotope fractionation may occur in HP blueschist-facies serpentinites (Debret et al., 2016). Deciphering the signatures of fluid–rock interactions in ophiolites can be relatively complex because these rocks often display various stages of fluid–rock interactions, fluid overprinting or polymetamorphism, especially in the case of subducted ophiolites. This study investigates non-traditional Fe and Ge isotope fractionation in ultrabasic (serpentinites) and basic rocks (amphibolite facies metagabbros) of the Limousin ophiolite (French Massif Central) that were not subducted during the Variscan orogeny. We aim to characterise the isotopic signatures of (sub-)seafloor hydrothermal alteration vs. magmatic processes and to understand processes controlling isotope fractionation during hydrothermal metamorphism in ancient non-subducted hydrothermally altered oceanic rocks.

## 2. Geological setting

The Limousin area is located in the northwestern French Massif Central. It is part of the European Variscan belt, which was formed by the Devonian to Carboniferous collision of Laurussia (formed by the assembly of Laurentia, Baltica and Avalonia continents) and Gondwana continents (Fig. 1a) (e.g. Lardeaux et al., 2014; Matte, 2001). Two main collision stages have been characterised in the Western Variscan belt. The Variscan orogeny was initiated during the Middle Devonian by the closure of the oceanic domains (including the Rheic ocean), which were opened during the Cambro-Ordovician rifting between the continental domains, and by the dislocation of the northern margin of the Gondwana (e.g.; Kroner and Romer, 2013; von Raumer et al., 2015). The collision between Laurussia and Gondwana-derived terranes occurred during the Early Carboniferous and was followed by Late Carboniferous orogenic collapse (Kroner and Romer, 2013; Lardeaux et al., 2014; Franke et al., 2017).

The western European Variscan belt is composed of three major domains (Fig. 1a): (1) the Rheno-Hercynian Zone (external domain), (2) the Saxothuringian Zone and, (3) the Moldanubian Zone (internal allochthonous domain) (e.g. Franke et al., 2017; Lardeaux et al., 2014). The allochthonous domain was formed by the superposition of nappes derived from peri-Gondwanan regions and includes a series of ophiolites and ophiolite-derived basic and ultrabasic rocks. (von Raumer et al., 2015, and references therein). In the Western Variscan

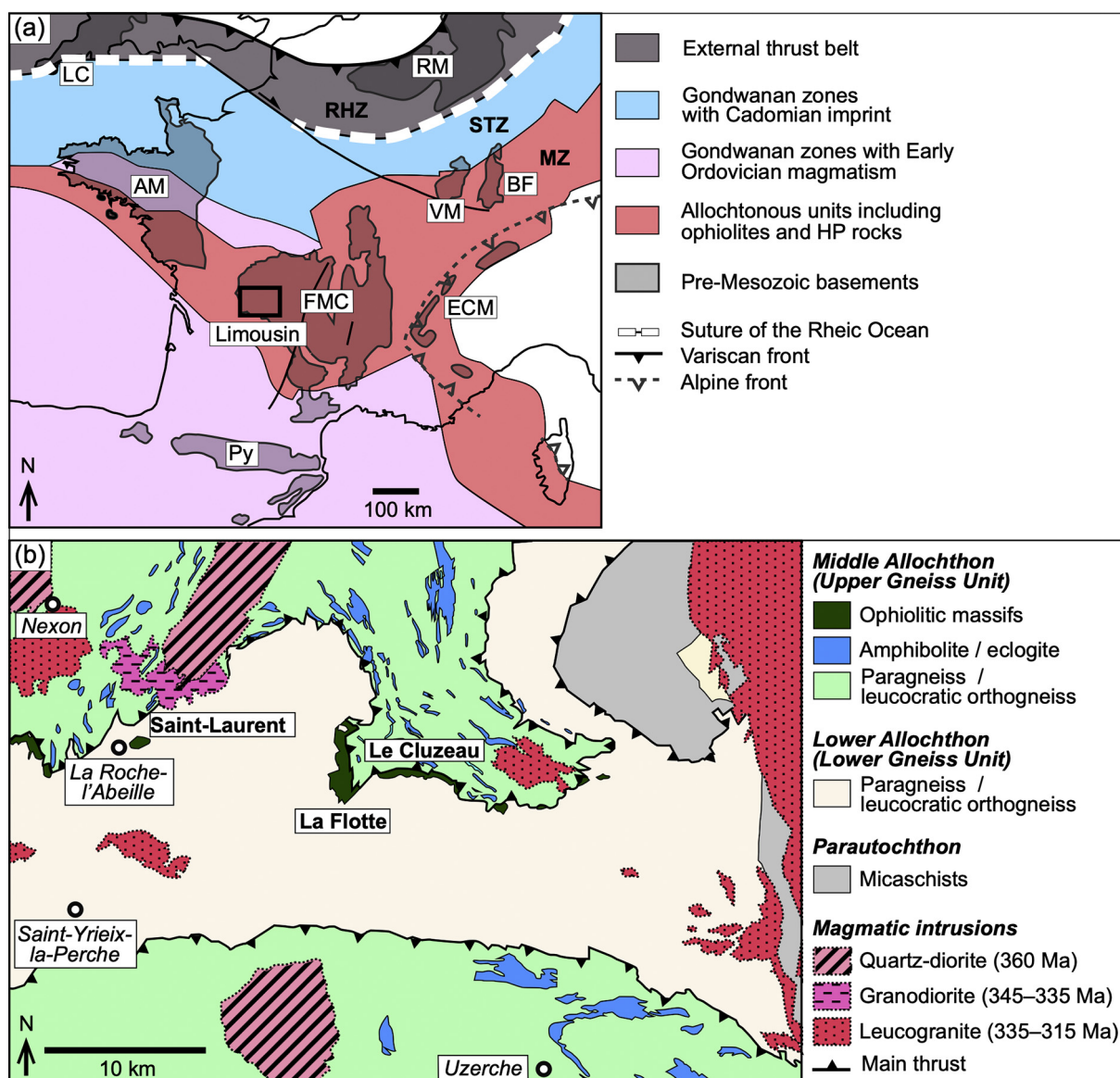


**Fig. 1.** Geological map of the studied area in the Limousin ophiolite (modified after Berger et al., 2005, 2010, and El Korh et al., 2019, 2020). AM, Armorican Massif; BF, Black Forest; ECM, External Crystalline Massifs of the Alps; FMC, French Massif Central; LC, Lizard Complex; Py, Pyrenees; RM, Rhenish Massif; VM, Vosges Massif; MZ, Moldanubian zone; RHZ, Rhenohercynian zone; STZ, Saxo-Thuringian zone.

belt, the emplacement of the ophiolite magmatic precursors along the Gondwana margin have been interpreted as the result of a late-Cambrian active margin (intra-continental back-arc basin rifting) that has followed the closure of the Proto-Rheic ocean during the Cambrian–Ordovician (von Raumer et al., 2015). Other studies consider the ophiolites as the remnants of a narrow ocean between Gondwana and Armorica named the “Galicia-South Brittany-Moldanubian” or “Medio-European” ocean (Matte, 2001; Faure et al., 2009; Lardeaux et al., 2014).

The FMC consists of a series of nappes, which were piled during the Devonian–Early Carboniferous, and display different units (Girardeau et al., 1986; Ledru et al., 1994; Faure et al., 2009). In the Limousin area, the Upper Allochthon (or Gartempe Unit) is formed by a series of low-grade Palaeozoic metasedimentary and metavolcanic associations (Fig. 1b). The Middle Allochthon (also known as the Upper Gneiss Unit), includes rocks from the “leptyno-amphibolite groups” (LAGs) (Santallier et al., 1988): paragneisses, leptynites and amphibolites of medium to high grade metamorphism, as well as migmatitic

metagreywackes and relicts of eclogites and granulites. The Lower Allochthon (also known as the Lower Gneiss Unit) is mainly composed of metasedimentary rocks (paragneisses, micaschists, metashales and metagreywackes), as well as Late Proterozoic–Early Cambrian and Ordovician leucocratic orthogneisses. The Parautochthon basement is composed of metasediments and metagranites.

Remnants of subducted ophiolites occur as lenses of HP–UHP eclogites (zoisite-eclogites and kyanite-eclogites; Berger et al., 2010), which crop out at the basis of the Middle Allochthon. U–Pb age data indicate that eclogites have recorded a protolith age of 475–489 Ma (zircon), indicating that their protoliths were emplaced during the Cambro-Ordovician rifting (Berger et al., 2010). The UHP event ( $P \sim 2.9 \pm 0.5$  GPa,  $T \sim 660 \pm 70$  °C) corresponds to a subduction at a depth of 100 km and is dated at  $412 \pm 5$  Ma (Berger et al., 2010).

The Limousin ophiolite belongs to the suite of oceanic rocks recognised in the Moldanubian Zone (von Raumer et al., 2015). It corresponds to a series of 1–5 km wide non-subducted ophiolite massifs, forming a 25 km long thrust sheet of basic and ultrabasic rocks in the



**Table 1**

Description, provenance and mineral assemblage of the studied samples.

Sample*	Rock type	Locality**	Mineralogical assemblage***
LAU-1	Serpentinite	Saint-Laurent	Serp-chl-spl-amph- $\pm$ ol- $\pm$ cpx
LAU-2	Serpentinite	Saint-Laurent	Serp-chl-spl-Fe ox
CLUZ-6	Serpentinite	Le Cluzeau	Serp-amph-chl-spl-Fe ox- Fe sulph
FLOT-2a	Serpentinite	La Flotte	Serp-spl-ol-Fe ox
FLOT-2b	Serpentinite	La Flotte	Serp-chl-spl-Fe ox
CLUZ-1	Amphibolite	Le Cluzeau	Amph-plag-Fe ox
CLUZ-1a	Amphibolite	Le Cluzeau	Amph-plag-Fe ox- $\pm$ chl
CLUZ-4	Amphibolite	Le Cluzeau	Amph-plag-ttn-Fe ox-Fe sulph- $\pm$ chl
CLUZ-5	Amphibolite	Le Cluzeau	Amph-plag-chl-Fe ox

\*Samples are from El Korh et al. (2019, 2020).

\*\*See Fig. 1.

\*\*\*The mineral abbreviations are from Kretz (1983); Fe sulph: Fe-sulphides (pyrite).

upper part of the Middle Allochthon (Dubuisson et al., 1989); Berger et al., 2005, 2006). The Limousin ophiolite has been interpreted as the plutonic sequence of a Iherzolite-harzburgite ophiolite type, emplaced in a slow-spreading mid-ocean ridge (Berger et al., 2006). The ophiolite bodies are composed of a series of serpentinised ultrabasic rocks and basic amphibolite-facies rocks, such as diopside-bearing harzburgites, harzburgites, dunites, wehrlites, harzburgites, troctolites, (meta)gabbros and amphibolites (Berger et al., 2005). Further to magma emplacement, the rocks were submitted to a pervasive sea-floor hydrothermal alteration under low-P conditions ( $\sim 0.2$  GPa), with temperature decreasing from high-T late-magmatic conditions to lower-T greenschist-zeolite metamorphic facies (Berger et al., 2005). The Limousin ophiolite-derived rocks have not been affected by a pervasive Variscan orogenic metamorphism, which probably

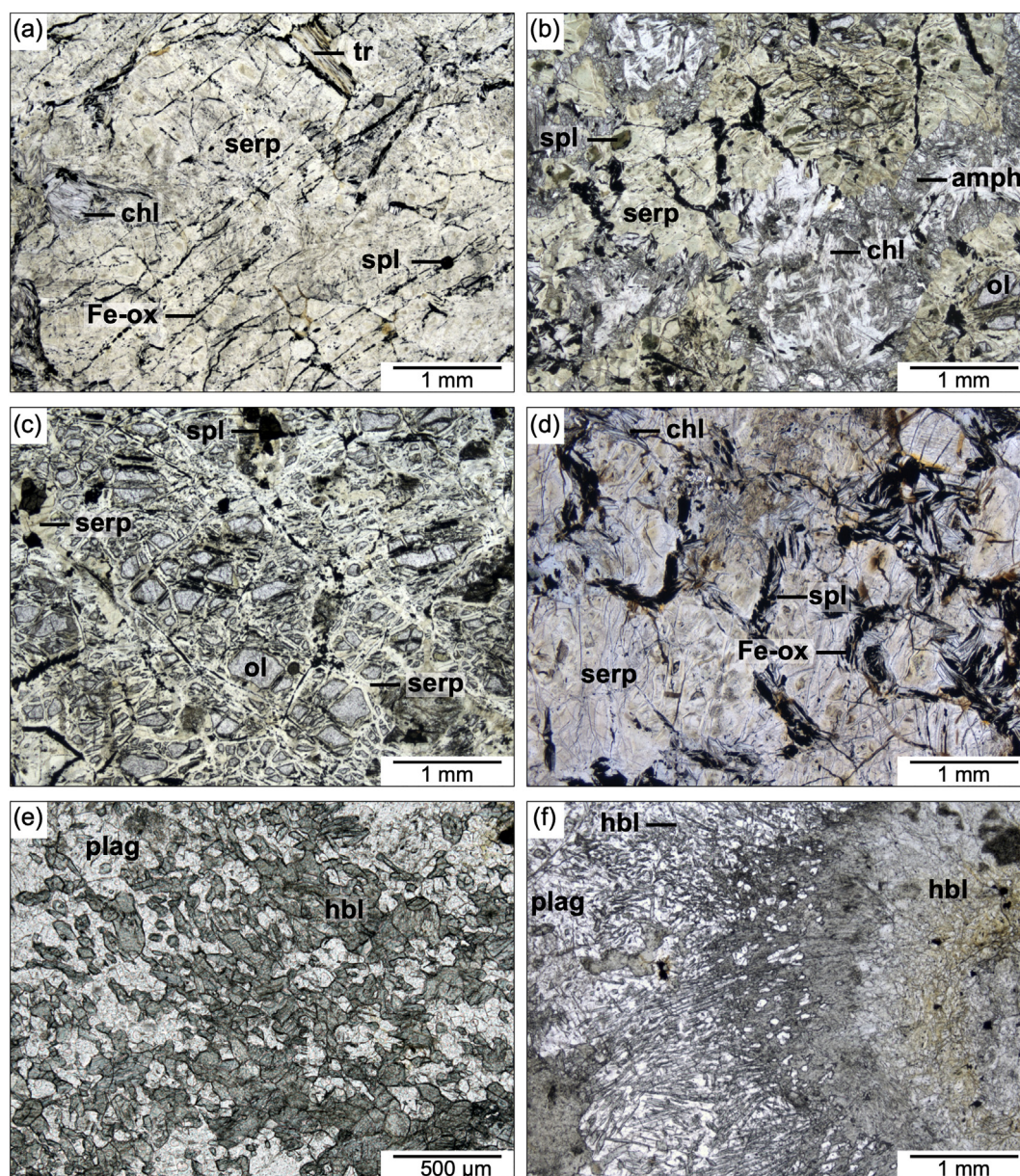


**Fig. 2.** Photomicrographs of the studied serpentinites (a–d) and amphibolites (e–f) from the Limousin ophiolite. (a) Serpentinite LAU2: ultrabasic protolith totally altered into serpentinite without relicts of magmatic minerals; serpentine (serp), tremolite (tr), chlorite (chl), spinel (spl). (b) Serpentinite CLUZ6: olivine (ol) replaced by serpentine. Serpentine is rimmed by coronas of amphibole (amph) (mainly tremolite) associated with chlorite and spinel. (c) Serpentinite FLOT2a: olivine partially to totally replaced by yellow serpentine. (d) Serpentinite FLOT2b: Replacement of the original magmatic minerals by serpentine, chlorite, spinel, and Fe-oxides. (e) Fine-grained amphibolite CLUZ1 slightly foliated and mainly consisting of plagioclase (plag) and hornblende (hbl) (f) Large-grained isotropic amphibolite CLUZ4: aggregates formed by large crystals of Mg-hbl replacing magmatic pyroxene. Amphibole aggregates are rimmed by plag-hbl symplectites and hbl needles.



**Table 2**  
Major and trace element composition of the studied samples.

Reference*		SiO <sub>2</sub>	Al <sub>2</sub> O <sub>3</sub> /SiO <sub>2</sub>	Fe <sub>2</sub> O <sub>3</sub> <sup>tot</sup>	MgO	CaO	Na <sub>2</sub> O	XMg	Fe <sup>3+</sup> /ΣFe	Cr	Ge	Rb	Ba	Y/Ti × 10 <sup>-3</sup>	(Ce/Yb) <sub>PM</sub> ***
		[1]	[1]	[1]	[1]	[1]	[1]	[1]	[1]	[2]	[2]	[2]	[2]	[1,2]	[2]
LAU1	Serpentinite	38.92	0.05	7.59	36.33	0.58	0.03	0.84	0.63	2793	0.88	bdl	9.4	bdl	bdl
LAU2	Serpentinite	38.62	0.04	7.48	36.06	0.03	bdl	0.84	0.71	3042	0.82	0.40	13	bdl	bdl
FLOT2a	Serpentinite	35.53	0.09	10.89	37.52	0.43	bdl	0.79	0.58	3427	0.89	0.45	8.7	1.61	0.47
FLOT2b	Serpentinite	35.39	0.12	10.33	34.74	0.07	bdl	0.79	0.67	2837	0.91	0.59	12	3.00	0.70
CLUZ6	Serpentinite	39.13	0.11	11.31	30.41	2.86	0.27	0.75	0.65	2436	1.2	0.88	14	3.56	0.40
CLUZ1	Amphibolite	48.06	0.38	6.61	10.24	12.43	1.84	0.63	0.13	958	1.2	1.9	23	3.95	0.60
CLUZ1a	Amphibolite	46.82	0.32	8.58	13.54	11.33	1.54	0.64	0.14	1120	1.4	1.7	23	4.13	0.63
CLUZ4	Amphibolite	49.23	0.33	5.28	11.11	13.85	1.42	0.70	0.11	859	1.4	1.9	14	4.33	0.66
CLUZ5	Amphibolite	48.26	0.33	7.68	10.94	11.74	2.07	0.61	0.13	906	1.4	2.9	27	3.55	0.62

Major elements in wt% oxides; trace elements in ppm; XMg = 100 × mol% MgO/(mol% MgO + mol% FeO<sub>tot</sub>).

bdl: below detection limit.

\* Raw data from: El Korh et al. 2019 [1]; El Korh et al. 2020 [2].

\*\* (Ce/Yb)<sub>PM</sub> normalised to the Primitive mantle (normalisation values are from Sun and McDonough 1989).

took place before nappe emplacement and accretion of ophiolite-derived rocks (Berger et al., 2005).

### 3. Studied samples

We have investigated the Fe and Ge isotopic compositions of five serpentinites (LAU1, LAU2, CLUZ6, FLOT2a, FLOT2b) and four amphibolite-facies basic rocks (CLUZ1, CLUZ1a, CLUZ4 and CLUZ5) from La Flotte, Le Cluzeau and Saint-Laurent ophiolite massifs (Fig. 1b; Table 1; see also El Korh et al., 2019, 2020).

The ultrabasic rocks are highly serpentinitised and have developed the typical mesh textures resulting from serpentinitisation at mid-ocean ridges (Bach et al., 2006; Viti and Mellini, 1998): brown Fe-rich core parts are rimmed by a second Fe-poorer yellow generation (El Korh et al., 2019) (Fig. 2a–d). Serpentinites from St-Laurent (LAU1, LAU2), which may correspond to the highly serpentinitised dunites described by Dubuisson et al. (1989), are composed of serpentine [XMg (= MgO/(MgO + FeO<sub>tot</sub>): 0.73–0.94; Fe<sup>3+</sup>/ΣFe (calculated by charge balance after microprobe analysis): 0.00–0.82], chlorite, amphibole (mainly tremolite; XMg: 0.79–0.92; Fe<sup>3+</sup>/ΣFe: 0.39–1.00), Cr-Fe-spinel (XMg: 0.02–0.08; Fe<sup>3+</sup>/ΣFe: 0.51–0.57), Fe-hydroxides and rare relicts of olivine (LAU1). Sample LAU1 contains a higher abundance of amphibole. In the serpentinites from Le Cluzeau (CLUZ6) and La Flotte (FLOT2a, FLOT2b), serpentine (XMg: 0.55–0.93; Fe<sup>3+</sup>/ΣFe: 0.0–1.0) have partially to totally replaced olivine, and is accompanied by amphibole (tremolite to Mg-hornblende; XMg: 0.83–0.88; Fe<sup>3+</sup>/ΣFe: 0.38–0.97), chlorite, spinel (Cr-Fe-spinels in sample CLUZ6 with XMg and Fe<sup>3+</sup>/ΣFe values of 0.03 and 0.37, respectively; Al-Fe-Cr-spinels in sample FLOT2a with XMg and Fe<sup>3+</sup>/ΣFe values of 0.32–0.53 and 0.12–0.24, respectively), iron oxides (magnetite) and sulphides. In sample CLUZ6, serpentine is rimmed by coronas of amphibole (mainly tremolite) associated with chlorite and spinel. This sample displays a texture similar to the serpentinitised troctolites described by Dubuisson et al. (1989) and Berger et al. (2005). However,

plagioclase is absent from sample CLUZ6, contrary to the samples from Berger et al. (2005), who described coronas made of amphibole, pyroxene and spinel and formed between serpentinitised olivine and plagioclase. Chlorite and amphibole abundance is variable in the samples from La Flotte. Alteration textures suggest that the samples from La Flotte correspond to serpentinitised harzburgites, while sample CLUZ6 may derive from a troctolite (Berger et al., 2005; Dubuisson et al., 1989) (Fig. 2). The serpentinites from Saint-Laurent show higher MgO contents, and lower contents of Fe<sub>2</sub>O<sub>3</sub><sup>tot</sup>, Al<sub>2</sub>O<sub>3</sub> and CaO than the serpentinites from La Flotte and Le Cluzeau (El Korh et al., 2019). All serpentinites have compatible and incompatible trace element compositions typical of the Primitive Mantle (Sun and McDonough, 1989), with high abundances in compatible transition metals (Sc, V, Cr, Co, Ni, Zn, Cu) and low contents of incompatible metals (Ge, Ga, Mo, Sn, Sb, W), Large-Ion Lithophile Elements (LILE: Cs, Rb, Ba), Li, Rare-Earth Elements (REE) and High Field Strength Element (HFSE: Th, U, Nb, Ta, Zr, Hf) abundances (El Korh et al., 2019, 2020). Serpentinites from Le Cluzeau and La Flotte display (Ce/Yb)<sub>PM</sub> ratios of 0.40 to 0.70, while serpentinites from St-Laurent have light REE (LREE) abundances below detection limit (El Korh et al., 2020). The temperature of hydrothermal alteration of ultrabasic rocks is estimated between 350 and 500 °C, because of the presence of tremolitic amphibole and the absence of talc (Berger et al., 2005). In particular, despite low Li abundances, δ<sup>7</sup>Li variations in the mineral assemblage of serpentinites have allowed to determine changes in hydrothermal

**Table 4**  
Iron isotopic compositions of Fe standards and studied samples.

Sample		n	$\delta^{56}\text{Fe}$ (‰)		$\delta^{57}\text{Fe}$ (‰)	
			Mean	$\pm 2\sigma^*$	Mean	$\pm 2\sigma^*$
PCC-1	Peridotite	7	+0.052	0.039	+0.091	0.055
Reference**						
[1]			+0.025	0.012	+0.053	0.018
LAU1	Serpentinite	3	+0.178	0.017	+0.234	0.054
LAU2	Serpentinite	2	+0.151	0.008	+0.213	0.030
FLOT2a	Serpentinite	2	+0.171	0.022	+0.281	0.041
FLOT2b	Serpentinite	3	+0.170	0.043	+0.221	0.048
CLUZ6	Serpentinite	2	+0.140	0.024	+0.198	0.042
CLUZ1	Amphibolite	4	+0.120	0.025	+0.162	0.027
CLUZ1a	Amphibolite	9	+0.117	0.028	+0.140	0.042
CLUZ4	Amphibolite	5	+0.158	0.040	+0.257	0.052
CLUZ5	Amphibolite	3	+0.029	0.033	+0.065	0.029

n = number of replicates;

δ<sup>56</sup>Fe values (‰) refer to IRMM-014 Fe standard normalisation;

\* 2σ uncertainties for the reference values of PCC-1 geostandard given as 95% confidence level; 2σ uncertainties for the measured PCC-1 geostandard and for the studied samples are given as 2σ standard error (= 2σ standard deviation /√n);

\*\* Reference values are from [1] Craddock and Dauphas (2011).

**Table 3**  
Oxygen isotopic compositions of the studied samples.

Sample		$\delta^{18}\text{O}$ (‰)
LAU1	Serpentinite	5.0
LAU2	Serpentinite	5.3
FLOT2a	Serpentinite	5.2
FLOT2b	Serpentinite	5.0
CLUZ6	Serpentinite	6.1
CLUZ1	Amphibolite	6.4
CLUZ1a	Amphibolite	6.5
CLUZ4	Amphibolite	6.2
CLUZ5	Amphibolite	6.6

**Table 5**  
Germanium isotopic compositions of Ge standards and studied samples.

Sample		n	$\delta^{72}\text{Ge}$ (‰)		$\delta^{73}\text{Ge}$ (‰)		$\delta^{74}\text{Ge}$ (‰)	
			Mean	$\pm 2\sigma^*$	Mean	$\pm 2\sigma^*$	Mean	$\pm 2\sigma^*$
Aldrich Reference**	Ge standard	12	−0.978	0.022 (se)	−1.468	0.053 (se)	−1.920	0.042 (se)
[1]			−1.05	0.15 (sd)	−1.58	0.27 (sd)	−2.04	0.23 (sd)
[2]			−1.03	0.12 (sd)	−1.54	0.17 (sd)	−2.01	0.23 (sd)
JMC Reference**	Ge standard	10	−0.139	0.023 (se)	−0.184	0.022 (se)	−0.280	0.055 (se)
[2]			−0.16	0.07 (sd)	−0.23	0.12 (sd)	−0.29	0.10 (sd)
LAU1	Serpentine	3	+0.400	0.033 (se)	+0.497	0.065 (se)	+0.792	0.097 (se)
LAU2	Serpentine	2	+0.285	0.016 (se)	+0.426	0.050 (se)	+0.574	0.038 (se)
FLOT2a	Serpentine	2	+0.353	0.069 (se)	+0.532	0.091 (se)	+0.703	0.066 (se)
FLOT2b	Serpentine	3	+0.469	0.046 (se)	+0.724	0.037 (se)	+0.934	0.028 (se)
CLUZ6	Serpentine	2	+0.246	0.060 (se)	+0.345	0.053 (se)	+0.481	0.049 (se)
CLUZ1	Amphibolite	4	+0.369	0.057 (se)	+0.581	0.013 (se)	+0.727	0.043 (se)
CLUZ1a	Amphibolite	9	+0.396	0.025 (se)	+0.554	0.058 (se)	+0.782	0.052 (se)
CLUZ4	Amphibolite	5	+0.351	0.013 (se)	+0.448	0.073 (se)	+0.735	0.032 (se)
CLUZ5	Amphibolite	3	+0.356	0.016 (se)	+0.486	0.031 (se)	+0.716	0.061 (se)

n = number of replicates;

$\delta^x\text{Ge}$  values (‰) refer to NIST3120a Ge standard normalisation;

\*  $2\sigma$  uncertainties for the reference values of Aldrich and JMC standards given as  $2\sigma$  standard deviations (sd);  $2\sigma$  uncertainties for the measured Aldrich and JMC standards and for the studied samples are given as  $2\sigma$  standard error (se) (=  $2\sigma$  standard deviation  $\sqrt{n}$ );

\*\* Reference values are from: [1] Luais (2012); [2] Escoubé et al. (2012).

alteration conditions, due to a temperature decrease and/or variations in the  $\delta^7\text{Li}$  composition (El Korh et al., 2019).

Two types of amphibolites were studied: fine-grained slightly foliated amphibolites (CLUZ1 and CLUZ1a) and isotropic amphibolites (CLUZ4 and CLUZ5), which derive from layered and isotropic gabbros, respectively (Berger et al., 2005). The two studied types of amphibolites are composed of green-brown amphibole (mainly hornblende with rare tremolite and pargasite), plagioclase, chlorite and iron oxides (magnetite, hematite; Fig. 2e–f). Rare magmatic plagioclase can be also observed.  $\text{Fe}^{3+}/\Sigma\text{Fe}$  and XMg values of amphibole vary between the studied samples ( $\text{Fe}^{3+}/\Sigma\text{Fe}$  of 0–0.34, 0.28–0.35 and 0.32–0.76 in samples CLUZ1–CLUZ1a, CLUZ4 and CLUZ5, respectively; XMg of 0.62–0.77, 0.69–0.80 and 0.62–0.70 in samples CLUZ1–CLUZ1a, CLUZ4 and CLUZ5, respectively). Ranges of  $\text{Al}_2\text{O}_3$  contents of amphibole overlap between foliated and isotropic amphibolites (3.17–14.37 and 1.58–12.64 wt.%, respectively). However, hornblende in foliated amphibolites often show higher  $\text{Al}_2\text{O}_3$  contents than hornblende in isotropic amphibolites (6.62–14.37 and 3.66–10.21 wt.%, respectively).

Berger et al. (2005) have described different types of amphiboles in amphibolites, plagioclase-bearing serpentinites and troctolites, mainly: 1) low-Al amphibole (mainly Mg-hornblende, actinolite and tremolite) from foliated and schistose amphibolites and; 2) Al-rich amphiboles (Mg-hornblende, pargasite, tschermakite) from symplectites around Al-poor amphiboles, from coronas between plagioclase and olivine and around clinopyroxene in troctolites, and from chlorite-rich amphibolites. Reaction textures and coronas are interpreted as the result of the reaction

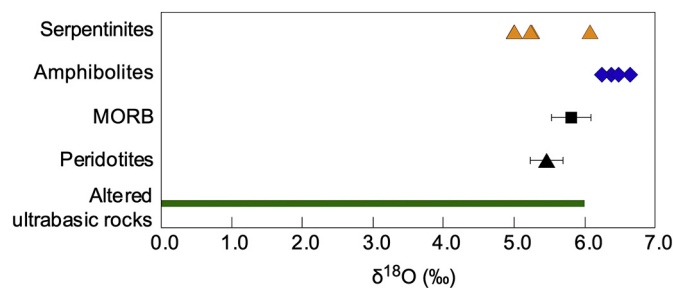


**Fig. 3.**  $\delta^{18}\text{O}$  variations in serpentinites and amphibolites from the Limousin ophiolite. Data for MORB, peridotites and altered ultrabasic rocks are from Muehlenbachs (1998), Matthey et al. (1994) and, Magaritz and Taylor (1974).

between olivine and plagioclase, which yielded an assemblage of orthopyroxene–clinopyroxene–spinel under low-P and high-T conditions hydrothermal metamorphism from late-magmatic conditions to greenschist facies temperatures (Berger et al., 2005).

Both studied amphibolite types display compatible and incompatible trace elements (including REE and HFSE and transition metals) typical of MORB (Sun and McDonough, 1989), with  $(\text{Ce}/\text{Yb})_{\text{PM}}$  ratio of 0.60 to 0.66. Only the LILE, Li, Pb and Sr abundances are slightly higher than N-MORB, which can suggest mobile element enrichment during hydrothermal alteration. Actually, amphibolites have Li abundances and  $\delta^7\text{Li}$  typical of hydrothermally altered sheeted dykes and gabbros that have interacted with heavy-Li fluids (seawater or upwelling hydrothermal fluids) under high-T conditions (El Korh et al., 2019). Equilibration between amphibole and plagioclase in amphibolites has occurred between c. 570 and 750 °C during high-T hydrothermal alteration (Berger et al., 2005).

Table 2 summarises the  $\text{SiO}_2$ ,  $\text{Al}_2\text{O}_3$ ,  $\text{Fe}_2\text{O}_3^{\text{tot}}$ , XMg,  $\text{Na}_2\text{O}$ , CaO, Cr, Ge, Rb and Ba concentrations, as well as the  $\text{Al}_2\text{O}_3/\text{SiO}_2$ , Y/Ti,  $(\text{Ce}/\text{Yb})_{\text{PM}}$  and  $\text{Fe}^{3+}/\Sigma\text{Fe}$  ratios (El Korh et al., 2019, 2020), that will be discussed below.

## 4. Analytical techniques

### 4.1. O isotopes

The oxygen isotope compositions of whole rocks were determined in the Stable Isotope Laboratory of the Institute of Earth Surface Dynamics (IDYST), University of Lausanne. Oxygen was extracted from 2 to 3 mg of rock powder using a 10 W New Wave  $\text{CO}_2$  laser and  $\text{F}_2$  gas. Isotopic composition of extracted oxygen was analysed with a Thermo-Finnigan MAT 253 gas source mass spectrometer.  $\delta^{18}\text{O}$  values are expressed in ‰ relative to VSMOW (Vienna Standard Mean Ocean Water) and are corrected to the LS\_1 quartz standard (in-house standard of the University of Lausanne; 18.1‰). The LS\_1 standard was analysed to monitor data accuracy and reproducibility (daily average value:  $+18.02 \pm 0.322\text{‰}$ ;  $n = 2$ ) (Table 3).

### 4.2. Fe isotopes

The whole rock Fe isotope compositions were measured in liquid mode by multi-collector inductively coupled plasma mass spectrometry (MC-ICP-MS) at the CRPG-Nancy using a NeptunePlus spectrometer (ThermoFisher Scientific, Germany and USA), following the procedure

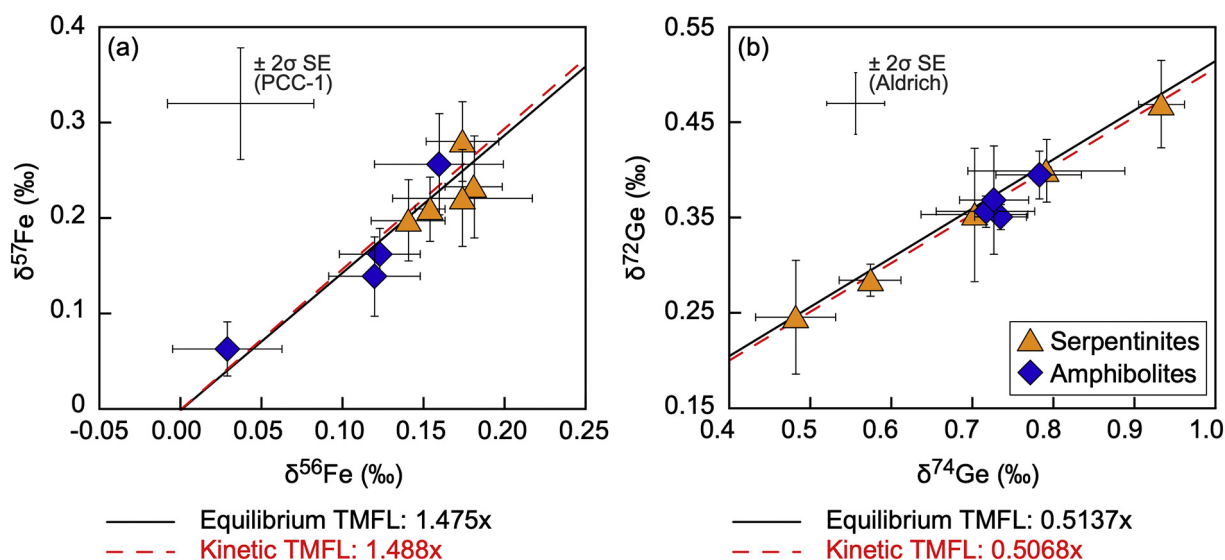


**Fig. 4.**  $\delta^{57}\text{Fe}_{\text{IRMM-014}}$  vs.  $\delta^{56}\text{Fe}_{\text{IRMM-014}}$  (a) and  $\delta^{72}\text{Ge}_{\text{NIST3120a}}$  vs.  $\delta^{74}\text{Ge}_{\text{NIST3120a}}$  (b) diagrams in serpentinites and amphibolites. Error bars are at  $2\sigma$  SE external reproducibility, based on replicate analyses. All Fe and Ge isotopic data plot within uncertainty along their respective equilibrium and kinetic theoretical mass fractionation lines (TMFL). For Fe isotopes:  $\delta^{57}\text{Fe}_{\text{IRMM-014}} = (1/m^{57}\text{Fe} - 1/m^{54}\text{Fe}) / (1/m^{56}\text{Fe} - 1/m^{54}\text{Fe}) \times \delta^{56}\text{Fe}_{\text{IRMM-014}} \approx 1.475 \times \delta^{56}\text{Fe}_{\text{IRMM-014}}$  (equilibrium TMFL) and  $\delta^{57}\text{Fe}_{\text{IRMM-014}} = [\ln(m^{57}\text{Fe}/m^{54}\text{Fe}) / \ln(m^{56}\text{Fe}/m^{54}\text{Fe})] \times \delta^{56}\text{Fe}_{\text{IRMM-014}} \approx 1.488 \times \delta^{56}\text{Fe}_{\text{IRMM-014}}$  (kinetic TMFL). For Ge isotopes:  $\delta^{72}\text{Ge}_{\text{NIST3120a}} = (1/m^{72}\text{Ge} - 1/m^{70}\text{Ge}) / (1/m^{74}\text{Ge} - 1/m^{70}\text{Ge}) \times \delta^{74}\text{Ge}_{\text{NIST3120a}} \approx 0.5137 \times \delta^{74}\text{Ge}_{\text{NIST3120a}}$  (equilibrium TMFL) and  $\delta^{72}\text{Ge}_{\text{NIST3120a}} = [\ln(m^{72}\text{Ge}/m^{70}\text{Ge}) / \ln(m^{74}\text{Ge}/m^{70}\text{Ge})] \times \delta^{74}\text{Ge}_{\text{NIST3120a}} \approx 0.5068 \times \delta^{74}\text{Ge}_{\text{NIST3120a}}$  (kinetic TMFL). Long-term reproducibility at  $2\sigma$  SE for the Fe PCC-1 geo-standard and for the Ge Aldrich standard are represented as error bars.

described in Liu et al. (2014) and El Korh et al. (2017a). Fe was separated according to the following chemical procedure: c. 10 mg of powdered samples were dissolved in three steps using: 1) a 2:1 mixture of HF (28 N) and  $\text{HNO}_3$  (15 N) on a hot plate at 90 °C; 2)  $\text{HNO}_3$  (15 N) at 60 °C; and 3) HCl (7 N) at 60 °C. After sample centrifugation, Fe was isolated through AG-MP-1 resin-exchange chromatography columns. Fractions were eluted with HCl (2 N) and dried down. Fe recovery is 88–99%. The dry fractions were then dissolved in  $\text{HNO}_3$  (7 N) and dried down, before being re-dissolved in  $\text{HNO}_3$  (0.05 N) for MC-ICP-MS analyses.

The MC-ICP-MS instrument was equipped with a standard nebuliser and cyclonic chamber, as well as Ni skimmer and sampler cones in standard geometrical configuration. In order to solve argide polyatomic interferences on Fe masses ( $^{40}\text{Ar}^{14}\text{N}$  on  $^{54}\text{Fe}$ ;  $^{40}\text{Ar}^{16}\text{O}$  on  $^{56}\text{Fe}$ ;  $^{40}\text{Ar}^{16}\text{O}^1\text{H}$  on  $^{57}\text{Fe}$ ), analyses were performed in static mode at a high resolution ( $M/\Delta M \approx 8000$ ) on the left side (low mass) of the Fe peaks. The cup configuration consisted of: Low 3 ( $^{53}\text{Cr}$ ), Low 2 ( $^{54}\text{Fe}$ ), Axial ( $^{56}\text{Fe}$ ) and High 1 ( $^{57}\text{Fe}$ ).  $^{53}\text{Cr}$  was used for the correction of the isobaric interference between  $^{54}\text{Cr}$  and  $^{54}\text{Fe}$  intensities. Gas flow rates, torch parameters and ion lenses were optimised by measurement of the IRMM-014 ultra-pure Fe standard. Prior to optimising the peak shapes and centring, the correction coefficients between the Faraday cups were determined by gain calibration. Analyses were carried out on 2–5 ppm Fe solutions, diluted in  $\text{HNO}_3$  (0.05 N). Analytical sequences consisted of 50 cycles (10 min in total), with 8 s integration time, after 13 min washout in  $\text{HNO}_3$  (0.5 N) and 8 min washout in  $\text{HNO}_3$  (0.05 N). Each sample analysis was sequentially bracketed by a measurement of the IRMM-014 standard. Fe isotope compositions are reported in ‰ standard delta values ( $\delta^{56}\text{Fe}$  and  $\delta^{57}\text{Fe}$ ), relative to the IRMM-014 standard.

Data bulk external reproducibility and accuracy were estimated by replicate analyses of the PCC-1 peridotite (Austin Creek, California, USA) geostandard (USGS) which was submitted to the same chemical and analytical procedure as the samples. The mean  $\delta^{56}\text{Fe}$  and  $\delta^{57}\text{Fe}$  values are within uncertainty with the data reported in the literature (Table 4).

#### 4.3. Ge isotopes

The whole rock Ge isotope ratios were measured using the Neptune Plus spectrometer MC-ICP-MS at the CRPG-Nancy (Table 5). Ge dissolution and separation followed the chemical procedure given in Luais

(2012). The powdered samples (c. 300 mg) were dissolved in a 3:1 mixture of HF (28 N) and  $\text{HNO}_3$  (15 N) at 60–65 °C, because of the strong Ge volatility. Several steps of leaching with HF and centrifugation allowed Ge recovery in the supernatant fraction (Luais 2012). Ge was isolated using two types of resin-exchange chromatography columns: 1) a AG 1-X8 anion exchange resin (chloride form, 200–400 mesh, 2 ml) with HF (1 N), where the Ge fraction was collected with  $\text{HNO}_3$  (0.2 N); 2) an AG 50 W-X8 (hydrogen form, 200–400 mesh, 2 ml cationic-exchange resin, where Ge was eluted with  $\text{HNO}_3$  (0.5 N) (Ge recovery: ~100%) (Luais 2012). Ge isotope analyses were carried out on 10 ppb diluted Ge standards and samples in  $\text{HNO}_3$  (0.01 N). Standards and samples were doped with the NBS SRM 994 Ga reference international isotopic standard ( $^{69}\text{Ga}/^{71}\text{Ga} = 1.50676$ ; Machlan et al., 1986), in a 10:1 ratio to monitor mass bias accuracy and instrumental drift during the analytical session.

The MC-ICP-MS spectrometer was equipped with a hydride generator introduction system (HGIS) to increase the sensitivity (Florin et al., 2020). Samples are mixed with a high-reducing solution of  $\text{NaBH}_4$ -NaOH in excess, which allows conversion of volatile aqueous species ( $\text{GeOH}_4$ ) to gaseous ( $\text{GeH}_4$ ) hydride species (Dedina and Tsalev 1995), with a yield of 100%. Isobaric interferences that do not form hydrides (such as argides, Zn, NiO, and FeO) are thus neutralised. Analyses were performed in static mode at a low resolution ( $M/\Delta M = 400$ ), with Ni skimmer and sampler cones placed in standard geometrical configuration. The cup configuration consisted of: Low 3 ( $^{68}\text{Zn}$ ), Low 2 ( $^{69}\text{Ga}$ ), Low 1 ( $^{70}\text{Ge}$ ), Axial ( $^{71}\text{Ga}$ ), High 1 ( $^{72}\text{Ge}$ ), High 2 ( $^{73}\text{Ge}$ ), High 3 ( $^{74}\text{Ge}$ ).  $^{68}\text{Zn}$  was used to correct the isobaric interference between  $^{70}\text{Ge}$  and  $^{70}\text{Zn}$  mathematically. Gas flow rates, torch parameters and ion lenses were optimised by measurement of the NIST SRM 3120a ultra-pure Ge standard (Luais 2012). The correction coefficients between the Faraday cups were calculated by a gain calibration before optimising peak shapes.

Analyses were carried out on 2–4 ppm Fe solutions, diluted in  $\text{HNO}_3$  (0.05 N). Analytical sequences consisted of 60 integration cycles (9 min in total), after 200 s washout in  $\text{HNO}_3$  (0.6 N) and 8 + 2 min washout in  $\text{HNO}_3$  (0.01 N). Each sample measurement was sequentially bracketed by a measurement of the NIST SRM 3120a standard. Ge isotope compositions are expressed in ‰ standard delta values ( $\delta^{72}\text{Ge}$ ,  $\delta^{73}\text{Ge}$  and  $\delta^{74}\text{Ge}$ ), relative to the NIST SRM 3120a standard.



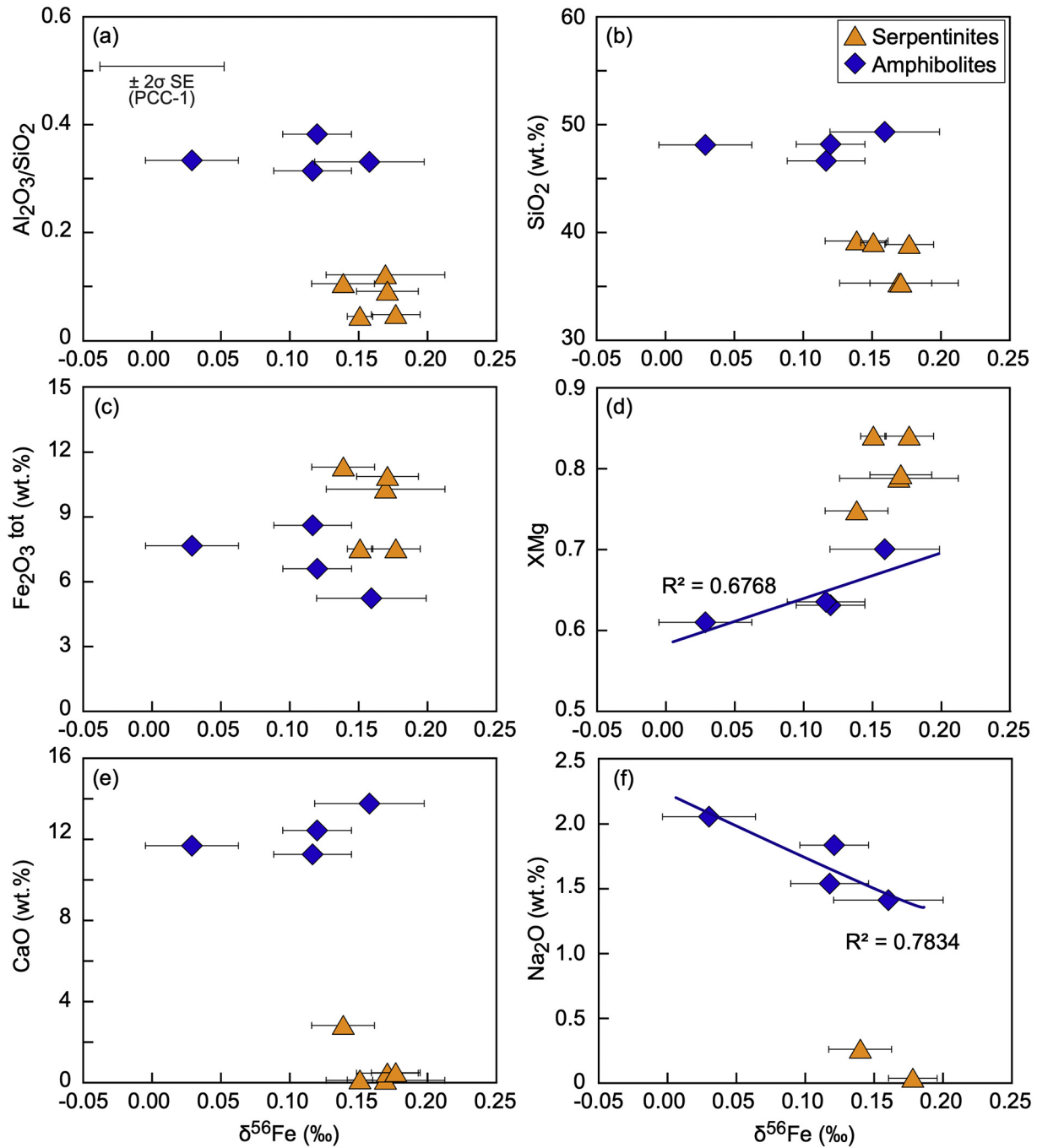


**Fig. 5.** (a–f)  $\text{Al}_2\text{O}_3/\text{SiO}_2$ ,  $\text{SiO}_2$ ,  $\text{Fe}_2\text{O}_3^{\text{tot}}$ ,  $\text{XMg}$ ,  $\text{CaO}$  and  $\text{Na}_2\text{O}$  vs.  $\delta^{56}\text{Fe}$  variations in the studied samples. In panels d and f, the correlation coefficient  $R^2$  is given for the whole series of amphibolites, as well as for the three samples that correlate well with the  $\delta^{56}\text{Fe}$  (excluding sample CLUZ1a). Error bars are at  $2\sigma$  SE external reproducibility.

The long-term stability of the ICP mass spectrometer, the external reproducibility and accuracy of the measurements were estimated by replicate analyses of the JMC and Aldrich Ge solution standards. The average  $\delta^{72}\text{Ge}$ ,  $\delta^{73}\text{Ge}$  and  $\delta^{74}\text{Ge}$  values (Table 5) are consistent with their respective reference values (Escoubé et al., 2012; Luais 2012).

## 5. Results

### 5.1. O isotopes

O isotope compositions of the studied serpentinites, amphibolites and UHP eclogite samples are given in Table 3. Serpentinites from Saint-Laurent and La Flotte have  $\delta^{18}\text{O}$  values varying between +5.0 and +5.3‰. The serpentinite from Le Cluzeau (CLUZ6) shows a higher

$\delta^{18}\text{O}$  of 6.1‰. Amphibolites have  $\delta^{18}\text{O}$  values ranging from +6.2 to +6.6‰ (Fig. 3).

### 5.2. Fe isotopes

The Fe isotopic compositions of the studied serpentinites, amphibolites and UHP eclogite are given in Table 4. The reproducibility on  $\delta^{56}\text{Fe}$  for all samples is generally lower than  $\pm 0.043\text{‰}$  at  $2\sigma$  SE. All data plot within uncertainty on the slope of the equilibrium and kinetic theoretical mass fractionation lines in a  $\delta^{57}\text{Fe}$  vs.  $\delta^{56}\text{Fe}$  diagram (Fig. 4a). The  $\delta^{56}\text{Fe}$  values of serpentinites vary between +0.14 and +0.18‰ (Fig. 4a). Amphibolites have  $\delta^{56}\text{Fe}$  values varying from +0.03 to +0.16‰, within the same range as serpentinites. The two groups of amphibolite facies rocks can be distinguished, even if their  $\delta^{56}\text{Fe}$  ranges

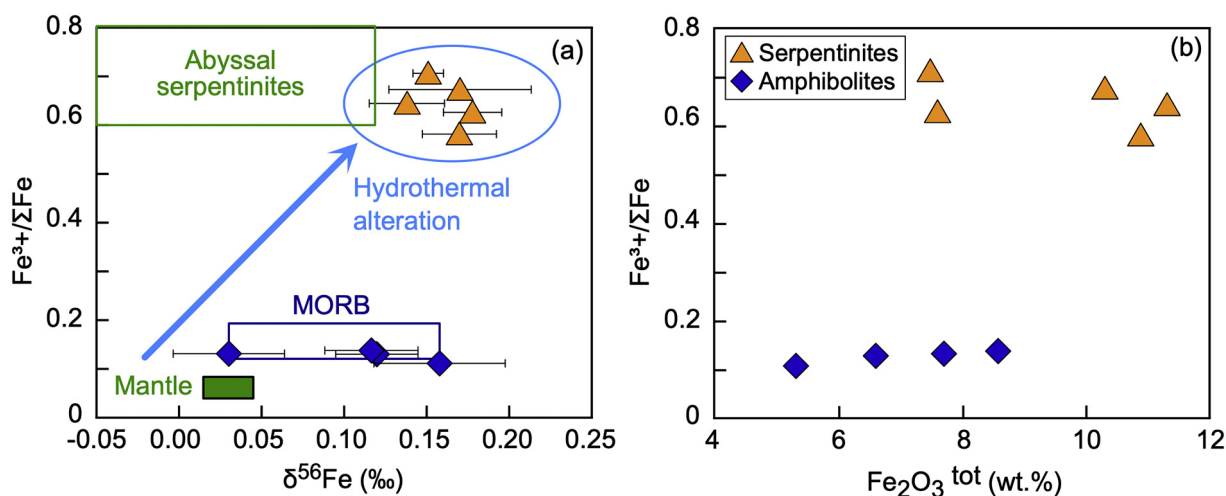


**Fig. 6.**  $\text{Fe}^{3+}/\Sigma\text{Fe}$  vs.  $\delta^{56}\text{Fe}$  (a) and  $\text{Fe}^{3+}/\Sigma\text{Fe}$  vs.  $\text{Fe}_2\text{O}_3^{\text{tot}}$  (b) variations in the studied samples. Error bars are at  $2\sigma$  SE external reproducibility. Data for abyssal serpentinites, mantle and MORB are from: Christie et al. (1986); Rouxel et al. (2003); Mével (2003); Weyer and Ionov (2007); Dauphas et al. (2009); Cottrell and Kelley (2011); Craddock and Dauphas, 2011; Craddock et al. (2013); Teng et al. (2008, 2013); Debret et al. (2014, 2016).

overlap: the  $\delta^{56}\text{Fe}$  of metamorphosed dykes do not vary from one sample to the other ( $+0.12\%$ ), while the metagabbros display heterogeneous  $\delta^{56}\text{Fe}$  values ( $+0.03$  to  $+0.16\%$ ) (Fig. 4a).

In serpentinites, the  $\delta^{56}\text{Fe}$  does not vary with  $\text{SiO}_2$ ,  $\text{Fe}_2\text{O}_3^{\text{tot}}$ , CaO, Cr and Ge concentrations, nor with XMg,  $\text{Al}_2\text{O}_3/\text{SiO}_2$ , Y/Ti,  $\text{Fe}^{3+}/\Sigma\text{Fe}$  and  $(\text{Ce}/\text{Yb})_{\text{PM}}$  ratios (Figs. 5, 6 and 7). By contrast, the  $\delta^{56}\text{Fe}$  displays a good negative correlation with the Ba content (Fig. 7f).

In amphibolites, the  $\delta^{56}\text{Fe}$  values do not correlate with  $\text{SiO}_2$ , Ni, Cr, and Ge contents, nor with  $\text{Al}_2\text{O}_3/\text{SiO}_2$ ,  $\text{Fe}^{3+}/\Sigma\text{Fe}$  and  $(\text{Ce}/\text{Yb})_{\text{PM}}$  values (Figs. 5, 6 and 7). The  $\delta^{56}\text{Fe}$  shows a good negative correlation with the  $\text{Fe}_2\text{O}_3^{\text{tot}}$  content only in 3 samples (Fig. 5c), while the  $\text{Fe}^{3+}/\Sigma\text{Fe}$  only varies slightly with the  $\text{Fe}_2\text{O}_3^{\text{tot}}$  content (Fig. 6b). The  $\delta^{56}\text{Fe}$  also increases with the increase of XMg and Y/Ti (Figs. 5 and 7), and with the decrease of  $\text{Na}_2\text{O}$ , Ba and Rb (Figs. 5f and 7e–f). While there is no clear correlation between  $\delta^{56}\text{Fe}$  and CaO values, the highest  $\delta^{56}\text{Fe}$  is measured in sample that shows the highest CaO abundance (CLUZ4; Fig. 5e).

### 5.3. Ge isotopes

The Ge isotopic compositions of the studied samples are presented in Table 5. All samples have a reproducibility on  $\delta^{74}\text{Ge}$  lower than  $\pm 0.097\%$  at  $2\sigma$  SE. All data plot within uncertainty on the slope of the equilibrium and kinetic theoretical mass fractionation lines in a  $\delta^{72}\text{Ge}$  vs.  $\delta^{74}\text{Ge}$  diagram (Fig. 4b). Serpentinites have  $\delta^{74}\text{Ge}$  values ranging from  $+0.48$  and  $+0.93\%$  that are similar to heavier than the values measured in ultrabasic rocks and MORB (Fig. 8). Amphibolites display a narrow range of  $\delta^{74}\text{Ge}$  values varying from  $+0.72$  to  $+0.78\%$ , similar within uncertainty to the heaviest values measured in basalts (Fig. 8).

In serpentinites, the  $\delta^{74}\text{Ge}$  displays a poor negative correlation with  $\text{SiO}_2$ , as well as a good positive correlation with the  $(\text{Ce}/\text{Yb})_{\text{PM}}$  ratio (3 samples out of 5). The  $\delta^{74}\text{Ge}$  does not show any correlation with CaO,  $\text{Fe}_2\text{O}_3^{\text{tot}}$ , Ni, Cr, Ge, concentrations, nor with  $\text{Al}_2\text{O}_3/\text{SiO}_2$ , XMg and  $\text{Fe}^{3+}/\Sigma\text{Fe}$  ratio (Figs. 8 and 9). Because of the narrow range of  $\delta^{74}\text{Ge}$  values in amphibolites, no correlation can be observed with major and trace element concentrations (Figs. 8 and 9).

## 6. Discussion: multi-isotope fractionation during hydrothermal alteration

### 6.1. O, Fe and Ge isotopic composition of serpentinites

Oxygen isotope fractionation in the oceanic lithosphere is strongly sensitive to hydrothermal alteration processes which can be distinguished by their distinct signatures (Cartwright and Barnicoat 1999;

Muehlenbachs 1998). The oxygen isotopic composition of the Limousin serpentinites is typical of peridotites ( $+5.5 \pm 0.2\%$ ; Matthey et al., 1994) and altered ultrabasic rocks (0 to  $+6\%$ ; Magaritz and Taylor, 1974) (Fig. 3). As the two ranges overlap, our data do not allow to determine whether O isotopes have fractionated during high-T hydrothermal alteration based on the  $\delta^{18}\text{O}$  alone. As serpentinites are strongly oxidised rocks ( $\text{Fe}^{3+}/\Sigma\text{Fe}$  from 0.58 to 0.71), the comparison of redox-sensitive isotopes, (such as Fe and Ge isotopes; Polyakov and Mineev 2000; Pokrovsky et al., 2014) with oxygen isotopes are expected to decipher magmatic and hydrothermal signatures in serpentinites.

Serpentinites have  $\text{Fe}_2\text{O}_3^{\text{tot}}$  contents (7.4–11.3%) and  $\text{Fe}^{3+}/\Sigma\text{Fe}$  typical of greenschist facies serpentinites in ophiolites (e.g. Debret et al., 2014, 2016). Iron isotopic compositions of serpentinites ( $+0.14$  to  $+0.18\%$ ) are within the range of MORB values (Sossi et al., 2016; Teng et al., 2013), but heavier than the values measured in partially to totally serpentinised abyssal peridotites ( $-0.10\%$  to  $+0.11\%$ ; Craddock et al., 2013; Debret et al., 2016) (Fig. 10). The absence of correlation between the  $\delta^{56}\text{Fe}$ ,  $\text{SiO}_2$ ,  $\text{Al}_2\text{O}_3/\text{SiO}_2$ , and the fluid-immobile trace elements Cr, Y/Ti and  $(\text{Ce}/\text{Yb})_{\text{PM}}$  ratio, as well as the correlation between the  $\delta^{56}\text{Fe}$  and Ba content, suggests that  $\delta^{56}\text{Fe}$  variations in serpentinites do not reflect the protolith signature but Fe isotope fractionation during hydrothermal alteration (Figs. 5, 6 and 7). There is no evidence of Fe leaching or addition during hydrothermal alteration and Fe oxidation, even if a weak correlation appears between  $\text{Fe}_2\text{O}_3^{\text{tot}}$  content and  $\text{Fe}^{3+}/\Sigma\text{Fe}$  values (Fig. 6b). However, Fe oxidation during hydrothermal alteration of the peridotite protoliths co-occurred with the precipitation of micrometric to nanometric  $\text{Fe}^{3+}$ -rich oxides (magnetite) and hydroxides (brucite) intercalated within serpentine (Bach et al., 2006; Viti and Mellini 1998). These alteration products preferentially incorporate heavy Fe isotopes (Polyakov and Mineev 2000), resulting in an increase of the  $\delta^{56}\text{Fe}$  of serpentinites. The good negative correlation between  $\delta^{56}\text{Fe}$  and  $\delta^{18}\text{O}$  values in serpentinites ( $R^2 = 0.75$ ) indicates synchronous O and Fe isotope fractionation during hydrothermal alteration (Fig. 11a).

Debret et al. (2016) observed a  $\delta^{56}\text{Fe}$  increase with increasing Fe-reducing conditions in HP Alpine serpentinites at the transition from lizardite-serpentinites [mean:  $-0.02 \pm 0.14\%$ ;  $2\sigma$  standard deviation (SD)] to antigorite-serpentinites ( $\delta^{56}\text{Fe}$  from  $-0.011$  to  $+0.142\%$ ; mean:  $+0.08 \pm 0.11\%$ ;  $2\sigma$  SD). The authors suggested that dehydration reactions in subducted serpentinites might release oxidised sulfate-rich and/or hypersaline fluids transporting light-Fe as  $\text{Fe}(\text{II})\text{-SO}_x$  or  $\text{Fe}(\text{II})\text{-Cl}_2$  species along the mantle wedge. The  $\delta^{56}\text{Fe}$  composition of the Limousin serpentinites is comparable to the highest  $\delta^{56}\text{Fe}$  values measured in some blueschist-facies Alpine antigorite-serpentinites.

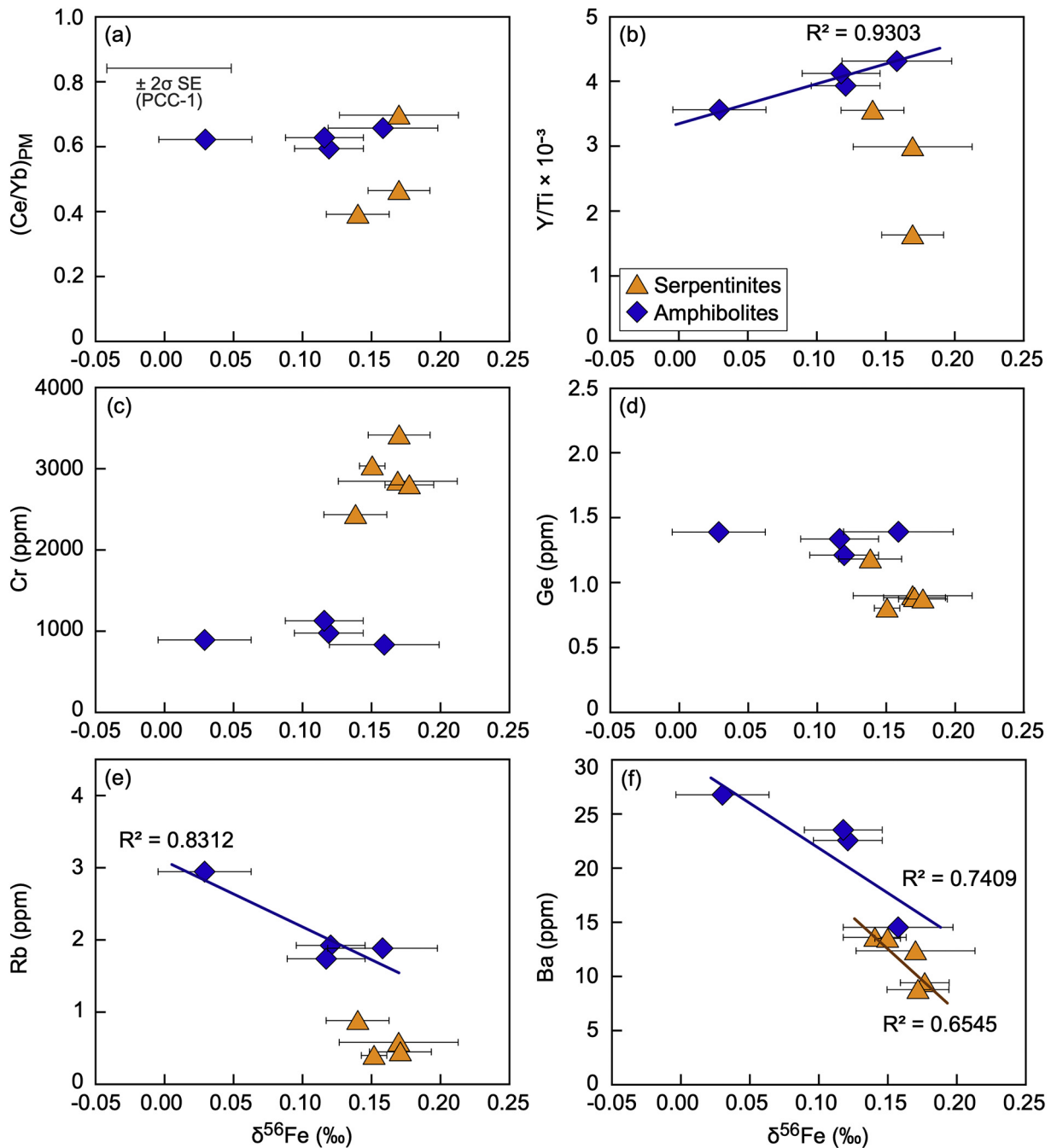


Fig. 7. (a–f)  $(\text{Ce/Yb})_{\text{PM}}$ , Y/Ti, Cr, Ge, Rb and Ba vs.  $\delta^{56}\text{Fe}$  variations in the studied samples. Error bars are at  $2\sigma$  SE external reproducibility.

However, our results contrast with previous studies, which suggest a conservative behaviour of Fe isotopes during ocean floor hydrothermal alteration of ultrabasic rocks into serpentinites (Craddock et al., 2013; Debret et al., 2016). The heterogeneous  $\delta^{56}\text{Fe}$  values of abyssal serpentinites is thought to reflect variations in the protolith composition, the isotopically heavier-Fe compositions being measured in pyroxene-rich and less depleted peridotites (Williams et al., 2005; Williams and Bizimis 2014). Debret et al. (2018) have observed that the light-Fe signature of Queyras ultrabasic rocks (i.e. Alpine serpentinites) does not correlate with fluid-immobile element ratios ( $\text{Al}_2\text{O}_3/\text{SiO}_2$  or Zr/Nb) and reflects mobilisation of Fe during prograde metamorphism. The high  $\delta^{56}\text{Fe}$  values measured in the Limousin serpentinites suggest that Fe isotopes may already fractionate towards heavier values during seafloor hydrothermal alteration in highly

oxidised abyssal serpentinites. Thus, subsequently subducted serpentinites may carry heavy-Fe up to the fore-arc mantle wedge and may contribute to mantle Fe heterogeneities. Indeed, large Fe isotope variations from  $-0.54$  to  $+0.16\%$  have been recorded by bulk mantle xenoliths (e.g. Poitrasson et al., 2013; Zhao et al., 2017).

Germanium isotopic compositions of serpentinites are similar to heavier than ultrabasic rocks ( $+0.46$  to  $+0.76\%$ ) and MORB ( $+0.55$  to  $+0.74\%$ ) (Rouxel et al., 2006; Escoubert et al., 2012, 2015; Luais 2012; Lalonde and Rouxel, unpublished); Rouxel and Luais 2017) (Fig. 12), suggesting Ge isotope fractionation during hydrothermal alteration at T between 350 and 500 °C. Besides, the increase of the  $\delta^{74}\text{Ge}$  values with the decrease of  $\text{SiO}_2$  and with the increase of the  $(\text{Ce/Yb})_{\text{PM}}$  ratio in serpentinites (Figs. 8 and 9) suggests that the Ge isotopic composition may be controlled by the protolith composition.



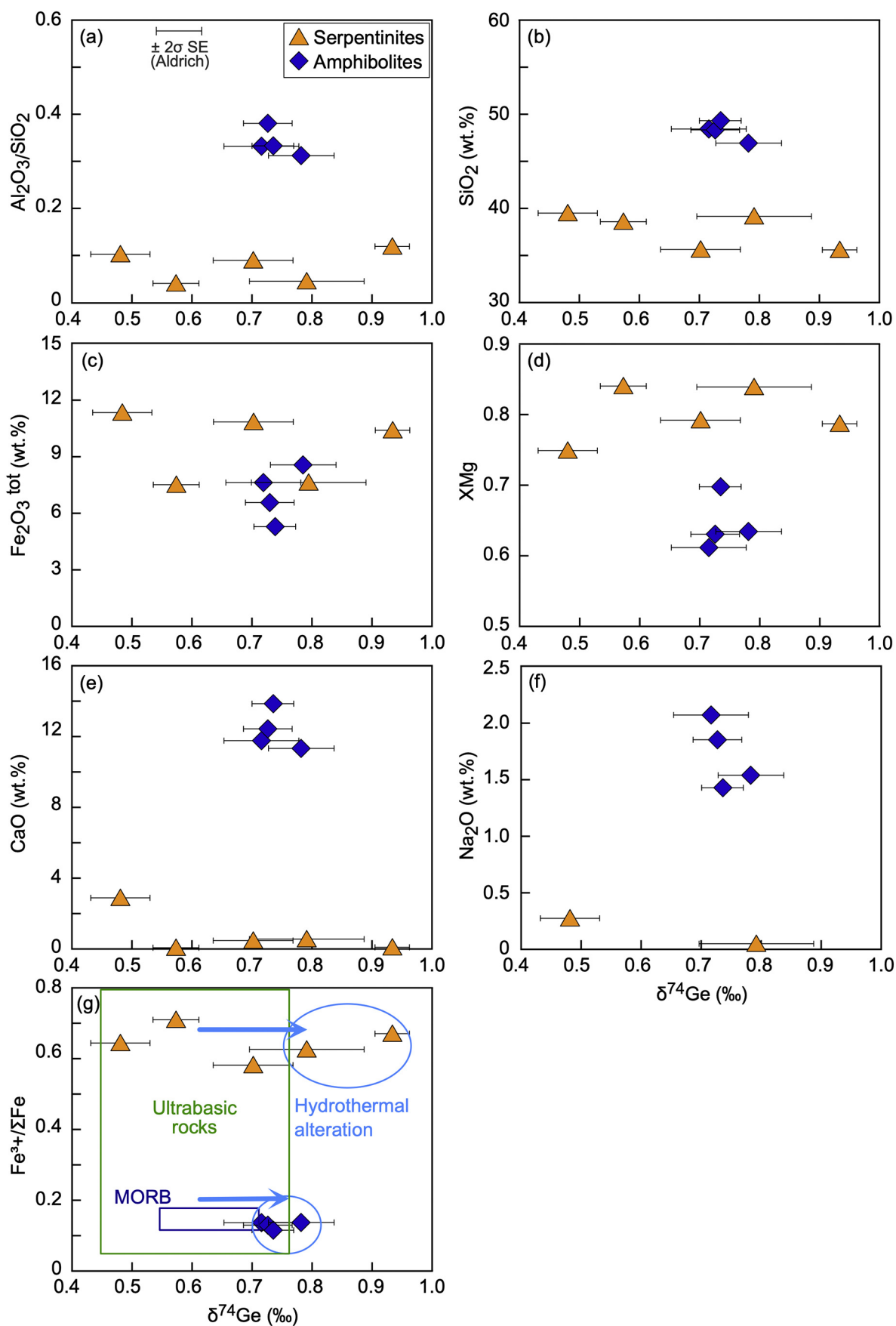


**Fig. 8.** (a–g)  $\text{Al}_2\text{O}_3/\text{SiO}_2$ ,  $\text{SiO}_2$ ,  $\text{Fe}_2\text{O}_3^{\text{tot}}$ , XMg, CaO,  $\text{Na}_2\text{O}$  and  $\text{Fe}^{3+}/\Sigma\text{Fe}$  vs.  $\delta^{74}\text{Ge}$  variations in the studied samples. Error bars are at  $2\sigma$  SE external reproducibility. Data for ultrabasic rocks and MORB are from: Christie et al. (1986); Mével (2003); Luais (2012); Escoubert et al. (2012, 2015); Cottrell and Kelley (2011); Debret et al. (2014); Rouxel and Luais (2017).

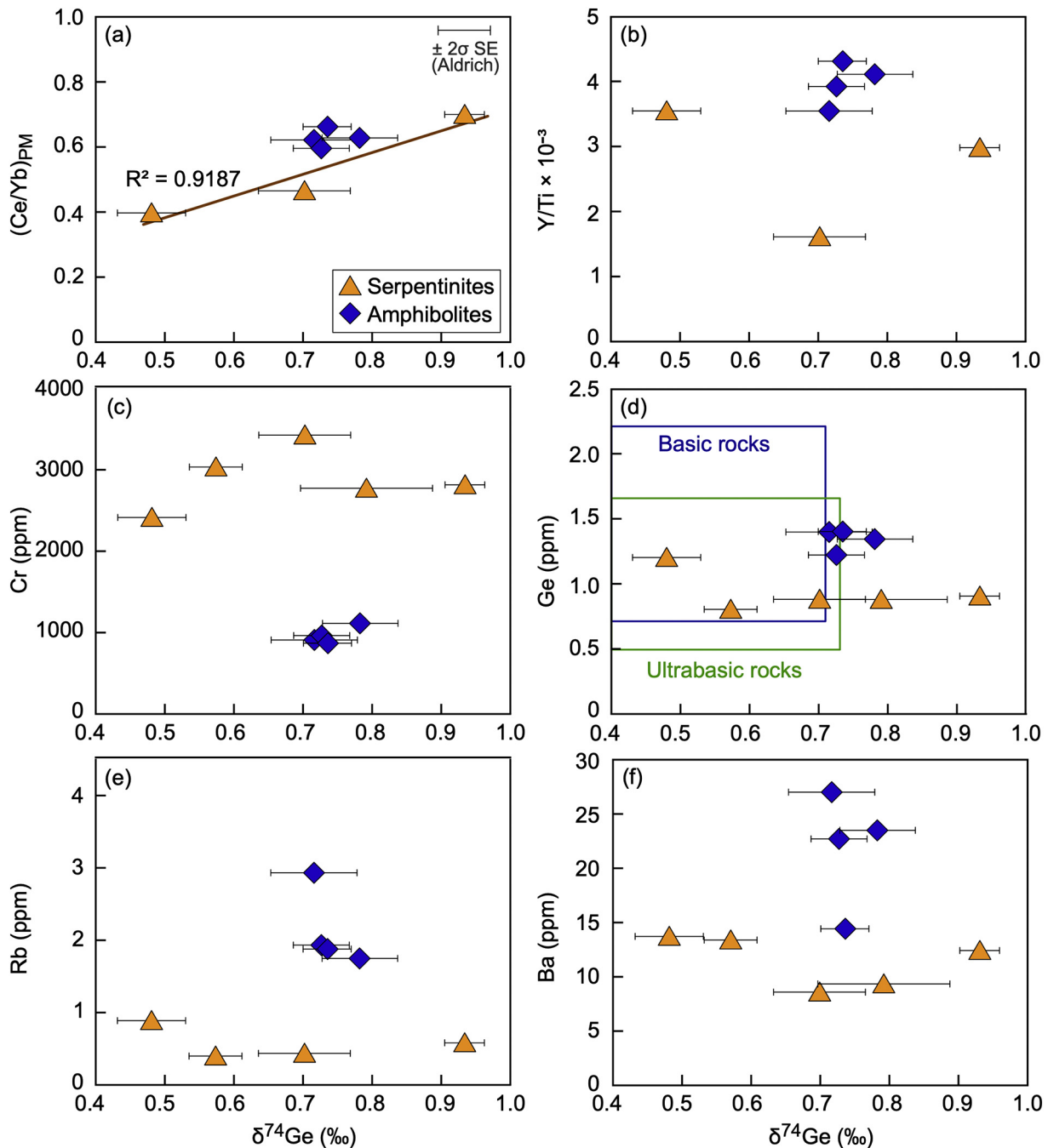


**Fig. 9.** (a–f) (Ce/Yb)<sub>PM</sub>, Y/Ti, Cr, Ge, Rb and Ba vs.  $\delta^{74}\text{Ge}$  variations in the studied samples. Error bars are at  $2\sigma$  SE external reproducibility. Data for ultrabasic and basic rocks are from: Luais (2012); Escoubé et al. (2012, 2015); Rouxel and Luais (2017); El Korh et al. (2017b).

Previous studies have shown that Ge isotope fractionation is strongly sensitive to low-T (<350 °C) hydrothermal processes. In particular, marine hydrothermal Fe-rich deposits display  $\delta^{74}\text{Ge}$  from  $-0.98$  to  $+0.16\%$ , while negative  $\delta^{74}\text{Ge}$  from  $-4.71$  to  $-2.98\%$  were measured in marine and terrestrial sulfide deposits (Belissont et al., 2014; Escoubé et al., 2012, 2015; Rouxel et al., 2006). Hydrothermal alteration can trigger Ge isotope fractionation towards heavier  $\delta^{74}\text{Ge}$  values in altered oceanic crust due to the interaction with heavy-Ge hydrothermal fluids and seawater (Escoubé et al., 2015; Rouxel et al., 2006). Moreover, Ge has a strong affinity with Fe hydroxides that precipitate during hydrothermal alteration, which can result in Ge isotope fractionation through Ge adsorption by goethite (Escoubé et al., 2015; Pokrovsky et al.,

2014). Consequently, the heavier  $\delta^{74}\text{Ge}$  values measured in serpentinites can be interpreted as the result of Ge isotope fractionation during hydrothermal alteration and oxidation of abyssal peridotites, while Ge isotopes may not have fractionated in the lighter samples.

The  $\delta^{74}\text{Ge}$  in serpentinites displays a good negative correlation with the  $\delta^{18}\text{O}$  ( $R^2 = 0.70$ ) and a good positive correlation with the  $\delta^{56}\text{Fe}$  ( $R^2 = 0.70$ ) (Figs. 13a and b), suggesting both Ge and Fe fractionation during hydrothermal alteration at T between 350 and 500 °C. However,  $\delta^{56}\text{Fe}$  values in serpentinites show a larger deviation from the values typically measured in ultrabasic rocks than  $\delta^{74}\text{Ge}$  and  $\delta^{18}\text{O}$  values. Hence, oxidising conditions have enhanced fractionation of Fe isotopes to a larger extent than Ge isotopes.

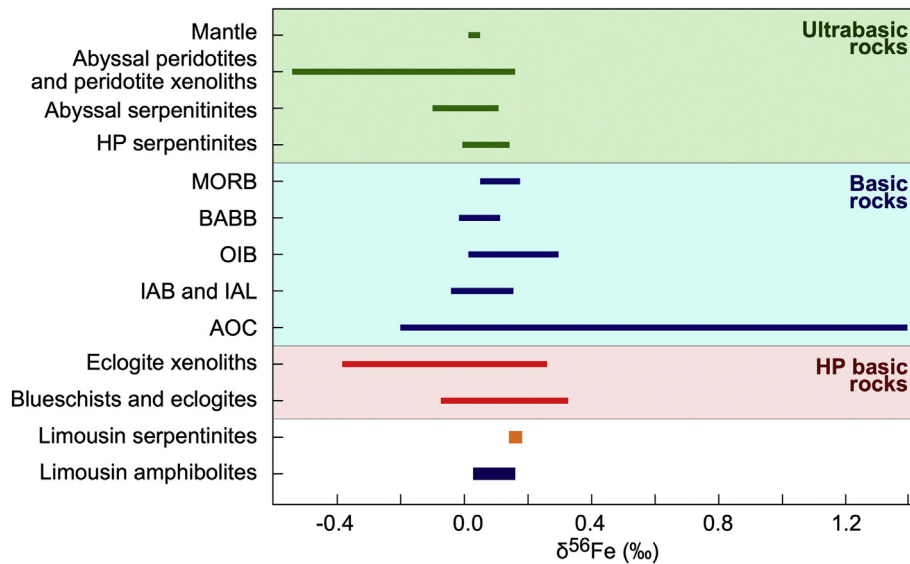


**Fig. 10.** Comparison of the  $\delta^{56}\text{Fe}$  isotope compositions of the Limousin samples with published values for ultrabasic and basic rocks. Data are from: Rouxel et al. (2003); Beard and Johnson (2004); Weyer and Ionov (2007); Schuessler et al. (2009); Williams et al. (2009); Dauphas et al. (2009); Craddock and Dauphas (2011); Sossi et al. (2012); Craddock et al. (2013); Teng et al. (2008, 2013); Poitrasson et al., 2013; Nebel et al. (2015); Konter et al. (2016); Debret et al. (2016); Li et al. (2016); Inglis et al. (2017); El Korh et al. (2017a); Zhang et al. (2019, 2020).

By contrast, the lowest  $\delta^{56}\text{Fe}$  and  $\delta^{74}\text{Ge}$  values and the highest  $\delta^{18}\text{O}$  value were measured in the sample from Le Cluzeau (CLUZ6), whose major element composition differs from the other serpentinites samples (higher  $\text{CaO}$  and  $\text{Fe}_2\text{O}_3^{\text{tot}}$  contents and lower  $\text{MgO}$  abundance). Contrary to the serpentinites from La Flotte and Saint-Laurent that derive from the alteration of abyssal peridotites, sample CLUZ6 probably derives from a troctolite. Thus, its isotopic signature also reflect a difference in the initial protolith composition in addition to hydrothermal alteration.

#### 6.2. O, Fe, and Ge isotope fractionation during high-temperature hydrothermal alteration in amphibolites

Amphibolites have  $\delta^{18}\text{O}$  values (+6.2 to +6.6‰) that are slightly higher than MORB, in agreement with the  $\delta^{18}\text{O}$  values measured in high-T hydrothermally altered basic rocks (Cartwright and Barnicoat 1999) (Fig. 3).  $\text{Fe}_2\text{O}_3^{\text{tot}}$  compositions of amphibolites (5.3–8.6%) are typical of oceanic gabbros (2.47–11.1%; Kaczmarek et al., 2008). Similarly, amphibolites  $\text{Fe}^{3+}/\Sigma\text{Fe}$  ratios (0.11–0.14) typical of MORB ( $\text{Fe}^{3+}/\Sigma\text{Fe} = 0.07\text{--}0.16$ ; Christie et al. 1986; Cottrell and Kelley 2011). In particular, sample CLUZ4, which displays symplectites made of anorthitic

plagioclase + hornblende, have conserved a MORB-like  $\delta^{56}\text{Fe}$  of  $+0.158 \pm 0.040\text{‰}$ . Symplectites and enrichment in Al and Mg were interpreted as the result of an interaction of preexisting amphibole or clinopyroxene with hot seawater-derived fluids, at temperature conditions of the amphibolite-to-greenschist facies transition rather than an effect of the Variscan orogenic metamorphism (see discussion in Berger et al., 2005). Thus, Fe appears to be relatively immobile during high-T hydrothermal alteration.  $\delta^{56}\text{Fe}$  values of amphibolites (+0.03 to +0.16‰) are within the range of MORB, despite a lower  $\delta^{56}\text{Fe}$  value measured in one of the metagabbro samples (CLUZ5) (Fig. 10). The  $\delta^{56}\text{Fe}$  increase with the  $\text{Fe}_2\text{O}_3^{\text{tot}}$  decrease and XMg and Y/TiO<sub>2</sub> increase argues that Fe isotopic composition reflects the protolith composition, despite an absence of correlation between the  $\delta^{56}\text{Fe}$  and SiO<sub>2</sub> and Al<sub>2</sub>O<sub>3</sub>/SiO<sub>2</sub> contents and between the  $\delta^{56}\text{Fe}$  and the fluid-immobile Cr and (Ce/Yb)<sub>PM</sub> ratio (Figs. 5 and 7). Assuming that Ba concentrations in amphibolites were not significantly modified by hydrothermal alteration, the negative correlation between  $\delta^{56}\text{Fe}$  and Ba values (Fig. 7f) may be caused by variations in the protolith composition as well, as Ba is compatible to mildly incompatible in plagioclase. By contrast, the  $\delta^{56}\text{Fe}$  decrease with the increase of Na<sub>2</sub>O, and Rb contents and with

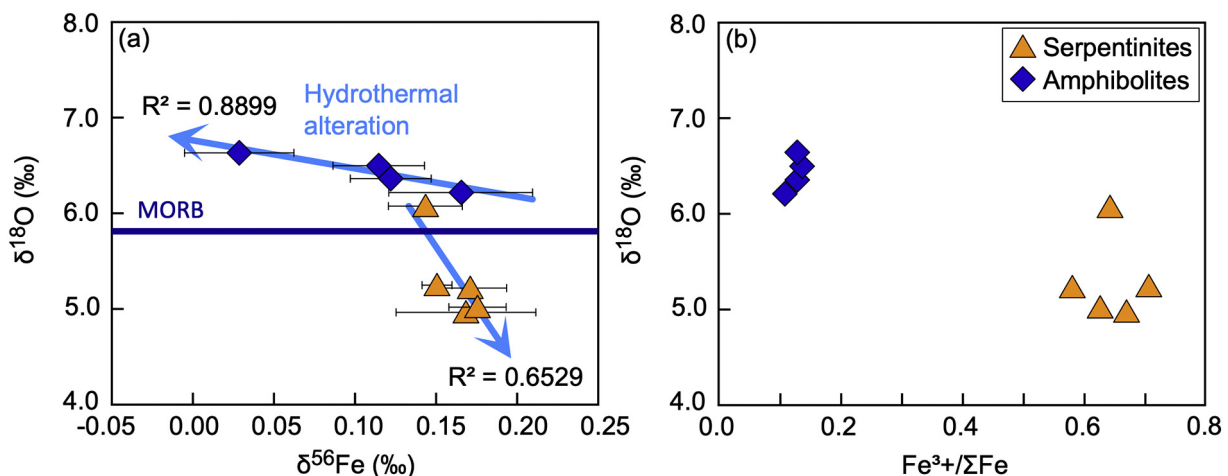


**Fig. 11.**  $\delta^{18}\text{O}$  vs.  $\delta^{56}\text{Fe}$  (a) and  $\delta^{18}\text{O}$  vs.  $\text{Fe}^{3+}/\Sigma\text{Fe}$  (b) in the studied serpentinites, amphibolites and UHP eclogite. Error bars are at  $2\sigma$  SE external reproducibility.



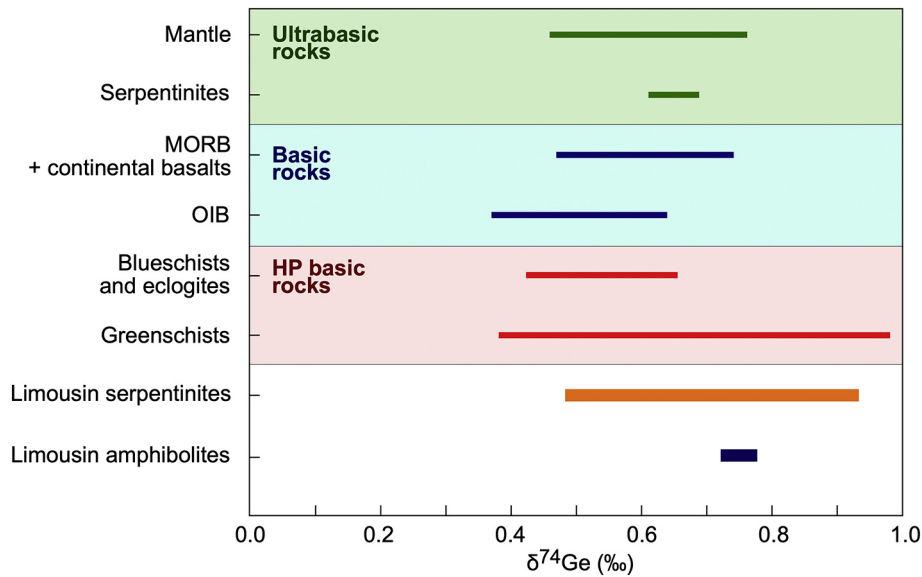


**Fig. 12.** Comparison of the  $\delta^{74}\text{Ge}$  isotope compositions of the Limousin samples with published values for ultrabasic and basic rocks. Data are from: Rouxel et al. (2006); Escoubé et al. (2012, 2015); Luais (2012); Lalonde and Rouxel (unpublished; cited by Rouxel and Luais 2017); Rouxel and Luais (2017); El Korh et al. (2017b).

the decrease of the CaO content, especially in the metagabbro CLUZ5, would suggest Fe isotope fractionation during hydrothermal alteration (Figs. 5 and 7). This hypothesis is supported by the good correlation between  $\delta^{56}\text{Fe}$  and  $\delta^{18}\text{O}$  values, despite the restricted range of Fe elemental and isotopic compositions and  $\delta^{18}\text{O}$  values (Fig. 11a). Similarly to serpentinites, a good correlation is observed between  $\delta^{56}\text{Fe}$  and  $\delta^{18}\text{O}$  values ( $R^2 = 0.87$ ): the  $\delta^{18}\text{O}$  increases with the decrease of the  $\delta^{56}\text{Fe}$ . Sample CLUZ5 is richer in chlorite than other amphibolites, where chlorite is only present as an accessory mineral (Table 1). Chlorite formation in metagabbro CLUZ5 indicates partial re-equilibration in the greenschist facies, and thus Fe isotope fractionation under lower temperature conditions of hydrothermal alteration. This contrasts with the positive correlations observed between Fe and O isotope composition in mantle-derived rocks and high-pressure metabasites (El Korh et al., 2017a; Williams et al., 2009). In the low-T hydrothermally altered metabasalts of the Ile de Groix, the  $\delta^{18}\text{O}$  increases with increasing the  $\delta^{56}\text{Fe}$  for each metamorphic facies (El Korh et al., 2017a). Different hypotheses were suggested to explain the coupled Fe and O isotope fractionation: 1) O and Fe fractionation did not occur concomitantly, with

O isotopes reflecting the hydrothermal signature, and Fe isotopes mirroring the protolith composition; 2) the different trends observed in eclogites, blueschists and greenschists result from different diffusion rates and kinetic isotope fractionation of Fe compared to O during hydrothermal processes; 3) the temperature of hydrothermal alteration was variable (El Korh et al., 2017a). Williams et al. (2009) interpreted the positive correlation between Fe and O isotopes in bulk mantle eclogite xenoliths from kimberlite pipes as the protolith composition inherited from variable isotope fractionation during disequilibrium partial melting. However, the correlation between  $\delta^{18}\text{O}$  and  $\delta^{57}\text{Fe}$  may also reflect intensive mantle metasomatism (Gréau et al., 2011).

Contrary to the highly oxidised serpentinites, high-T hydrothermal alteration in amphibolites did not trigger any Fe oxidation. This may be due to the precipitation of reduced  $\text{Fe}^{2+}$ -rich alteration products (sulphides) (Rouxel et al., 2003) or to the low permeability of gabbroic rocks, which prevents hydrothermal fluids to migrate (Cartwright and Barnicoat 1999). Moreover, the various degrees of Fe oxidation states and Fe isotope fractionation between amphibolites and serpentinites can be explained by the different temperature of hydrothermal

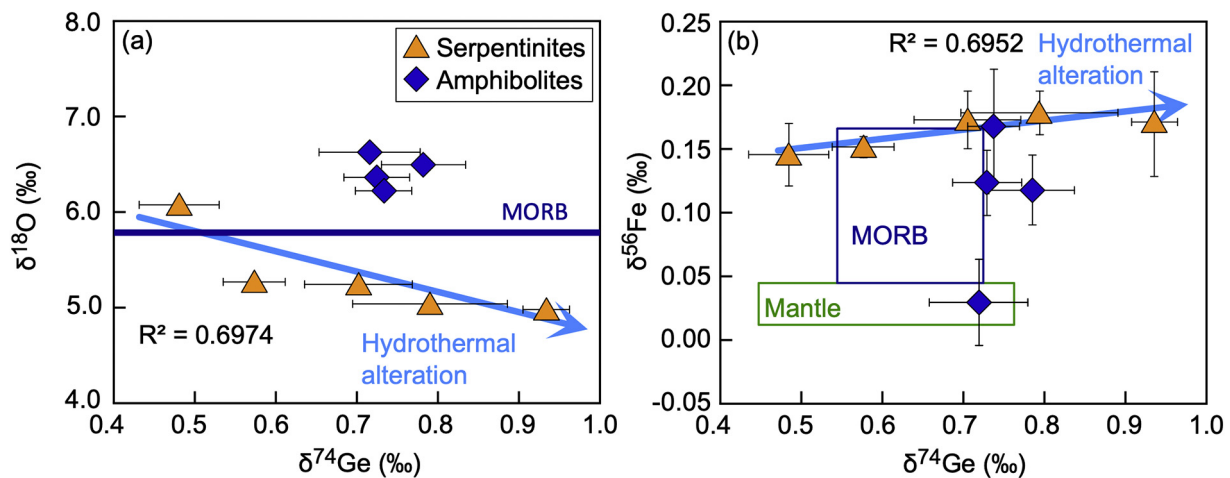


**Fig. 13.**  $\delta^{18}\text{O}$  vs.  $\delta^{74}\text{Ge}$  (a) and  $\delta^{56}\text{Fe}$  vs.  $\delta^{74}\text{Ge}$  (b) in the studied serpentinites, and amphibolites. Error bars are at  $2\sigma$  SE external reproducibility. Data for mantle and MORB are from: Weyer and Ionov (2007); Luais (2012); Teng et al. (2008, 2013); Dauphas et al. (2009); Craddock and Dauphas, 2011; Escoubé et al. (2012, 2015); Craddock et al. (2013); Debret et al. (2014); Rouxel and Luais (2017).

alteration, which was lower in serpentinites (350–500 °C) than in amphibolites (570–750 °C) (Berger et al., 2005).

Amphibolites show a small range of  $\delta^{74}\text{Ge}$  values (+0.72 to +0.77‰), that are heavier than most basalts and gabbros (+0.37 to +0.74‰; for a review, see Rouxel and Luais 2017) and than high-pressure metabasites (El Korh et al., 2017b) (Fig. 11). As observed for serpentinites, hydrothermal alteration of basic rocks may have been responsible for Ge isotope fractionation towards heavier values than their protolith. However, no  $\delta^{74}\text{Ge}$  vs.  $\delta^{56}\text{Fe}$  correlation is observed, as  $\delta^{56}\text{Fe}$  values in amphibolites do not differ significantly from the  $\delta^{56}\text{Fe}$  of basic rocks, while  $\delta^{74}\text{Ge}$  values show evidence of a definite deviation from the values typically measured in basic rocks (Fig. 13b). Hence, Ge isotope fractionation has prevailed over Fe isotope fractionation during hydrothermal alteration of basic rocks. Reducing conditions have enhanced Ge isotope fractionation towards compositions heavier than MORB. A similar behaviour has also been observed during fluid-rock interactions in the retrograde greenschist facies metabasites of the Ile de Groix: in the most retrogressed samples, rehydration reactions in a reducing context triggered Ge isotope fractionation towards heavy compositions compared to the more oxidised greenschists and high-grade facies rocks (El Korh et al., 2017b).

## 7. Concluding remarks

Three isotopic systems (O, Fe and Ge) were employed to investigate processes controlling isotope fractionation in ancient non-subducted hydrothermally altered oceanic rocks from the Limousin ophiolite. The two main lithologies (serpentinites and amphibolites) display variable O, Fe and Ge compositions. The ultrabasic and basic magmatic precursors of the Limousin ophiolite-derived rocks were significantly metasomatised during the pervasive hydrothermal alteration on sea-floor that has followed magma emplacement. While Fe and Ge isotopic signatures of pre-Variscan hydrothermal processes were preserved, there is no evidence of subsequent isotope fractionation during fluid-rock interactions related to the Variscan collision in the FMC, even during nappe stacking, involving ophiolite-derived rocks, under high-temperature conditions leading regional-scale partial melting.

In particular, Fe and Ge isotopes shows an opposite behaviour with contrasting redox conditions. In the highly oxidised abyssal serpentinites, Fe isotopes ( $\delta^{56}\text{Fe}$  from +0.14 to +0.18‰) may fractionate significantly towards heavier values than their magmatic ultrabasic protolith. By contrast, the  $\delta^{74}\text{Ge}$  (+0.48 to +0.93‰) only increases during intensive hydrothermal alteration of ultrabasic rocks. Amphibolite facies metagabbros, can conserve MORB-like Fe isotopic compositions (+0.12 to +0.16‰) during hydrothermal alteration, but the  $\delta^{56}\text{Fe}$  can decrease (+0.03‰) with the increase of the  $\delta^{18}\text{O}$  during intensive hydrothermal alteration. Ge isotopes can fractionate towards heavier values than basic protoliths in metagabbros (+0.72 to +0.78‰) that have conserved a MORB-like Fe reduced state during hydrothermal alteration. Hence, coupled O–Fe–Ge isotopes are efficient tracers of magmatic vs. hydrothermal processes.

## Declaration of Competing Interest

The authors declare that they have no known competing financial interests or personal relationships that could have appeared to influence the work reported in this paper.

## Acknowledgments

We thank Beatrice Luais for her contribution in Fe and Ge isotope data acquisition and for useful discussions, and Benita Putlitz for technical support with O isotope analyses. We also thank Etienne Deloule for constructive discussions. We thank two anonymous reviewers for their constructive comments which help to improve the manuscript. We also thank Xian-Hua Li for the editorial handling of our manuscript. The

research was financially supported by the University of Fribourg, the TelluS-SYSTER program from the Institut National des Sciences de l'Univers (INSU), and by the French National Research Agency through the national program "Investissements d'avenir" (ANR-10-LABX-21-LABEX RESSOURCES21).

## References

- Bach, W., Paulick, H., Garrido, C.J., Ildefonse, B., Meurer, W.P., Humphris, S.E., 2006. Unraveling the sequence of serpentinization reactions: petrography, mineral chemistry, and petrophysics of serpentinites from MAR 15°N (ODP Leg 209, Site 1274). *Geophys. Res. Lett.* 33, L13306. <https://doi.org/10.1029/2006GL025681>.
- Beard, B.L., Johnson, C.M., 2004. Inter-mineral Fe isotope variations in mantle-derived rocks and implications for the Fe geochemical cycle. *Geochim. Cosmochim. Acta* 68, 4727–4743.
- Beinlich, A., Klemd, R., John, T., Gao, J., 2010. Trace-element mobilization during metasomatism along a major fluid conduit: eclogitization of a blueschist as a consequence of fluid–rock interaction. *Geochim. Cosmochim. Acta* 74, 1892–1922.
- Belissant, R., Boiron, M.-C., Luais, B., Cathelineau, M., 2014. LA-ICP-MS analyses of minor and trace elements and bulk Ge isotopes in zoned Ge-rich sphalerites from the Noailhac – Saint-Salvy deposit (France): insights into incorporation mechanisms and ore deposition processes. *Geochim. Cosmochim. Acta* 126, 518–540.
- Bennett, S.A., Rouxel, O.J., Schmidt, K., Garbe-Schönberg, D., Statham, P.J., German, C.R., 2009. Iron isotope fractionation in a buoyant hydrothermal plume from the Mid-Atlantic Ridge at 5°S. *Geochim. Cosmochim. Acta* 73, 5619–5634.
- Berger, J., Féménias, O., Mercier, J.C.C., Demaiffe, D., 2005. Ocean-floor hydrothermal metamorphism in the Limousin ophiolites (western French Massif Central): evidence of a rare preserved Variscan oceanic marker. *J. Metamorph. Geol.* 23, 795–812.
- Berger, J., Féménias, O., Mercier, J.C.C., Demaiffe, D., 2006. A Variscan slow-spreading ridge (MOR-LHOT) in Limousin (French Massif Central): magmatic evolution and tectonic setting inferred from mineral chemistry. *Mineral. Mag.* 70, 175–185.
- Berger, J., Féménias, O., Ohnenstetter, D., Bruguière, O., Plissart, G., Mercier, J.C.C., Demaiffe, D., 2010. New occurrence of UHP eclogites in Limousin (French Massif Central): Age, tectonic setting and fluid–rock interactions. *Lithos* 118, 365–382.
- Bernstein, L.R., 1985. Germanium geochemistry and mineralogy. *Geochim. Cosmochim. Acta* 49, 2409–2422.
- Cartwright, I., Barnicoat, A.C., 1999. Stable isotope geochemistry of alpine ophiolites: a window to ocean floor hydrothermal alteration and constraints on fluid–rock interaction during high-pressure metamorphism. *Int. J. Earth Sci.* 88, 219–235.
- Christie, D.M., Carmichael, I.S.E., Langmuir, C.H., 1986. Oxidation states of mid-ocean ridge basalt glasses. *Earth Planet. Sci. Lett.* 79, 397–411.
- Cottrell, E., Kelley, K.A., 2011. The oxidation state of Fe in MORB glasses and the oxygen fugacity of the upper mantle. *Earth Planet. Sci. Lett.* 305, 270–282.
- Craddock, P., Dauphas, N., 2011. Iron isotopic compositions of geological reference materials and chondrites. *Geostand. Geoanal. Res.* 35, 101–123.
- Craddock, P.R., Warren, J.M., Dauphas, N., 2013. Abyssal peridotites reveal the near-chondritic Fe isotopic composition of the Earth. *Earth Planet. Sci. Lett.* 365, 63–76.
- Dauphas, N., Craddock, P.R., Asimow, P.D., Bennett, V.C., Nutman, A.P., Ohnenstetter, D., 2009. Iron isotopes may reveal the redox conditions of mantle melting from Archean to present. *Earth Planet. Sci. Lett.* 288, 255–267.
- Debret, B., Andreani, M., Muñoz, M., Bolfan-Casanova, N., Carlot, J., Nicollet, C., Schwartz, S., Trcera, N., 2014. Evolution of Fe redox state in serpentine during subduction. *Earth Planet. Sci. Lett.* 400, 206–218.
- Debret, B., Millet, M.A., Pons, M.L., Bouilhol, P., Inglis, E., Williams, H., 2016. Isotopic evidence for iron mobility during subduction. *Geology* 44, 215–218.
- Debret, B., Bouilhol, P., Pons, M.L., Williams, H., 2018. Carbonate transfer during the onset of slab delamination: new insights from Fe and Zn stable isotopes. *J. Petrol.* 59, 1145–1166.
- Dedina, J., Tsalav, D.L., 1995. *Hydride Generation, Atomic Absorption Spectrometry*. Wiley, Chichester, UK.
- Dubuisson, G., Mercier, J.-C.C., Girardeau, J., Frison, J.Y., 1989. Evidence for a lost ocean in Variscan terranes of the Western Massif Central, France. *Nature* 337, 729–732.
- El Korh, A., Luais, B., Deloule, E., Cividini, D., 2017a. Iron isotope fractionation in subduction-related high-pressure metabasites (Ile de Groix, France). *Contrib. Mineral. Petrol.* 172, 41.
- El Korh, A., Luais, B., Boiron, M.C., Deloule, E., Cividini, D., 2017b. Investigation of Ge and Ga exchange behaviour and Ge isotopic fractionation during subduction zone metamorphism. *Chem. Geol.* 449, 165–181.
- El Korh, A., Deloule, E., Luais, B., Boiron, M.C., Bastian, L., Vigier, N., 2019. Lithium behaviour and isotope fractionation during fluid–rock interactions in Variscan oceanic suture zones: Limousin ophiolite and Ile de Groix high-pressure terrane (France). *J. Petrol.* 60, 1963–1990.
- El Korh, A., Boiron, M.C., Cathelineau, M., Deloule, E., Luais, B., 2020. Tracing metallic pre-concentrations in the Limousin ophiolite-derived rocks and Variscan granites (French Massif Central). *Lithos* 356–357, 105345.
- Escoube, R., Rouxel, O., Luais, B., Ponzevera, E., Donard, O.F.X., 2012. Intercomparison study of germanium isotope composition of geological and reference materials. *Geostand. Geoanal. Res.* 36, 149–159.
- Escoube, R., Rouxel, O., Edwards, K., Glazer, B., Donard, O.F.X., 2015. Coupled Ge/Si and Ge isotope ratios as geochemical tracers of seafloor hydrothermal systems: case studies at Loihi Seamount and East Pacific rise 9°500 N. *Geochim. Cosmochim. Acta* 167, 93–112.
- Faure, M., Lardeaux, J.M., Ledru, P., 2009. A review of the pre-Permian geology of the Variscan French Massif Central. *Compt. Rendus Geosci.* 341, 202–213.

- Florin, G., Luais, B., Rushmer, T., Alard, O., 2020. Influence of redox processes on the germanium isotopic composition of ordinary chondrites. *Geochim. Cosmochim. Acta* 269, 270–291.
- Franke, W., Cocks, L.R.M., Torsvik, T.H., 2017. The Palaeozoic Variscan oceans revisited. *Gondwana Res.* 48, 257–284.
- Girardeau, J., Dubuisson, G., Mercier, J.-C.C., 1986. Cinématique de mise en place des ophiolites et nappes cristallophiliennes du Limousin, Ouest du Massif Central français. *Bullet. Soc. Géol. France* 2, 849–860.
- Gréau, Y., Huang, J.X., Griffin, W.L., Renac, C., Alard, O., O'Reilly, S.Y., 2011. Type I eclogites from Roberts Victor kimberlites: products of extensive mantle metasomatism. *Geochim. Cosmochim. Acta* 75, 6927–6954.
- Hill, P.S., Schauble, E.A., Young, E.D., 2010. Effects of changing solution chemistry on Fe3+/Fe2+ isotope fractionation in aqueous Fe–Cl solutions. *Geochim. Cosmochim. Acta* 74, 6669–6689.
- Inglis, E.C., Debret, B., Burton, K.W., Millet, M.A., Pons, M.L., Dale, C.W., Bouihol, P., Cooper, M., Nowell, G.M., McCoy-West, A., Williams, H.M., 2017. The behaviour of iron and zinc stable isotopes accompanying the subduction of mafic oceanic crust: a case study from Western Alpine Ophiolites. *Geochim. Geophys. Geosyst.* <https://doi.org/10.1002/2016GC006735>.
- Johnson, C., Beard, B., Weyer, S., 2020. *Iron Geochemistry: An Isotopic Perspective*. Springer Nature Switzerland AG.
- Kaczmarek, M.A., Müntener, O., Rubatto, D., 2008. Trace element chemistry and U–Pb dating of zircons from oceanic gabbros and their relationship with whole rock composition (Lanzo, Italian Alps). *Contrib. Mineral. Petrol.* 155, 295–312.
- Konter, J.G., Pietruszka, A.J., Hanan, B.B., Finlayson, V.A., Craddock, P.R., Jackson, M.G., Dauphas, N., 2016. Unusual  $\delta^{56}\text{Fe}$  values in Samoan rejuvenated lavas generated in the mantle. *Earth Planet. Sci. Lett.* 450, 221–232.
- Kretz, R., 1983. Symbols for rock-forming minerals. *Am. Mineral.* 68, 277–279.
- Kroner, U., Romer, R.L., 2013. Two plates—Many subduction zones: the Variscan orogeny reconsidered. *Gondwana Res.* 24, 298–329.
- Lardeaux, J.M., Schulmann, K., Faure, M., Janoušek, V., Lexa, O., Skrzypek, E., Edel, J.B., Štírká, P., 2014. The Moldanubian zone in the French Massif Central, Vosges/Schwarzwald and Bohemian Massif revisited: differences and similarities. *Geol. Soc. Lond. Spec. Publ.* 405, 7–44.
- Ledru, P., Autran, A., Santallier, D., 1994. Lithostratigraphy of Variscan terranes in the French Massif Central: A basis for paleogeographical reconstructions. In: Keppie, J.D. (Ed.), *Pre-Mesozoic Geology in France and Related Areas*. Springer-Verlag, Berlin Heidelberg, pp. 276–288.
- Li, X., Zhao, H., Tang, M., Liu, Y., 2009. Theoretical prediction for several important equilibrium Ge isotope fractionation factors and geological implications. *Earth Planet. Sci. Lett.* 287, 1–11.
- Li, D.Y., Xiao, Y.L., Li, W.Y., Zhu, X., Williams, H.M., Li, Y.L., 2016. Iron isotopic systematics of UHP eclogites respond to oxidizing fluid during exhumation. *J. Metamorph. Geol.* 34, 987–997.
- Liu, P.P., Zhou, M.F., Luais, B., Cividini, D., Rollier-Bard, C., 2014. Disequilibrium iron isotope fractionation during the high-temperature magmatic differentiation of the Baima Fe–Ti oxide-bearing mafic intrusion, SW China. *Earth Planet. Sci. Lett.* 399, 21–29.
- Luais, B., 2012. Germanium chemistry and MC-ICPMS isotopic measurements of Fe–Ni, Zn alloys and silicate matrices: Insights into deep Earth processes. *Chem. Geol.* 334, 295–311.
- Machlan, L.A., Gramlich, J.W., Powell, L.J., Lambert, G.M., 1986. Absolute isotope abundance ratio and atomic weight of a reference sample of gallium. *J. Res. Natl. Bureau Stand. A Phys. Chem.* 91, 323–331.
- Magaritz, M., Taylor, H.P., 1974. Oxygen and hydrogen isotope studies of serpentinization in Troodos Ophiolite complex, Cyprus. *Earth Planet. Sci. Lett.* 23, 8–14.
- Manning, C.E., 2004. The chemistry of subduction-zone fluids. *Earth Planet. Sci. Lett.* 223, 1–16.
- Matte, P., 2001. The Variscan collage and orogeny (480–290 Ma) and the tectonic definition of the Armorica microplate: a review. *Terra Nova* 13, 122–128.
- Mattey, D., Lowry, D., Macpherson, C., 1994. Oxygen isotope composition of mantle peridotite. *Earth Planet. Sci. Lett.* 128, 231–241.
- Mével, C., 2003. Serpentinization of abyssal peridotites at mid-ocean ridges. *Compt. Rendus Geosci.* 335, 825–852.
- Muehlenbachs, K., 1998. The oxygen isotopic composition of the oceans, sediments and the seafloor. *Chem. Geol.* 145, 263–273.
- Nebel, O., Arculus, R.J., Sossi, P.A., Jenner, F.E., Whan, T.H.E., 2013. Iron isotopic evidence for convective resurfacing of recycled arc-front mantle beneath back-arc basins. *Geophys. Res. Lett.* 40, 5849–5853.
- Nebel, O., Sossi, P.A., Bénard, A., Wille, M., Vroon, P.Z., Arculus, R.J., 2015. Redox-variability and controls in subduction zones from an iron-isotope perspective. *Earth Planet. Sci. Lett.* 432, 142–151.
- Poirasson, F., Delpech, G., Grégoire, M., 2013. On the iron isotope heterogeneity of lithospheric mantle xenoliths: implications for mantle metasomatism, the origin of basalts and the iron isotope composition of the Earth. *Contrib. Mineral. Petrol.* 165, 1243–1258.
- Pokrovski, G.S., Schott, J., 1998. Thermodynamic properties of aqueous Ge(IV) hydroxide complexes from 25 to 350 °C: implications for the behavior of germanium and the Ge/Si ratio in hydrothermal fluids. *Geochim. Cosmochim. Acta* 62, 1631–1642.
- Pokrovsky, O.S., Galy, A., Schott, J., Pokrovski, G.S., Mantoura, S., 2014. Germanium isotope fractionation during Ge adsorption on goethite and its coprecipitation with Fe oxy (hydr)oxides. *Geochim. Cosmochim. Acta* 131, 138–149.
- Polyakov, V.B., Mineev, S.D., 2000. The use of Mössbauer spectroscopy in stable isotope geochemistry. *Geochim. Cosmochim. Acta* 64, 849–865.
- Rouxel, O.J., Luais, B., 2017. Germanium isotope geochemistry. *Rev. Mineral. Geochem.* 82, 601–656.
- Rouxel, O., Dobbek, N., Ludden, J., Fouquet, Y., 2003. Iron isotope fractionation during oceanic crust alteration. *Chem. Geol.* 202, 155–182.
- Rouxel, O., Galy, A., Elderfield, H., 2006. Germanium isotopic variations in igneous rocks and marine sediments. *Geochim. Cosmochim. Acta* 70, 3387–3400.
- Rouxel, O., Shanks, W.C., Bach, W., Edwards, K.J., 2008. Integrated Fe- and S-isotope study of sea floor hydrothermal vents at East Pacific rise 9–10 N. *Chem. Geol.* 252, 214–227.
- Santallier, D., Briand, B., Ménot, R.P., Piboule, M., 1988. Les complexes leptynomphiboliques (C.L.A.): revue critique et suggestions pour un meilleur emploi de ce terme. *Bullet. Soc. Géol. France* 8 (4), 3–12.
- Schuessler, J.A., Schoenberg, R., Sigmarsson, O., 2009. Iron and lithium isotope systematics of the Hekla volcano, Iceland - Evidence for Fe isotope fractionation during magma differentiation. *Chem. Geol.* 258, 78–91.
- Sossi, P.A., O'Neill, H.S.C., 2017. The effect of bonding environment on iron isotope fractionation between minerals at high temperature. *Geochim. Cosmochim. Acta* 196, 121–143.
- Sossi, P.A., Foden, J.D., Halverson, G., 2012. Redox-controlled iron isotope fractionation during magmatic differentiation. *Contrib. Mineral. Petrol.* 164, 757–772.
- Sossi, P.A., Nebel, O., Foden, J.D., 2016. Iron isotope systematics in planetary reservoirs. *Earth Planet. Sci. Lett.* 452, 295–308.
- Su, B.X., Teng, F.Z., Hu, Y., Shi, R.D., Zhou, M.F., Zhu, B., Liu, F., Gong, X.H., Huang, Q.S., Xiao, Y., Chen, C., He, Y.S., 2015. Iron and magnesium isotope fractionation in oceanic lithosphere and sub-arc mantle: Perspectives from ophiolites. *Earth Planet. Sci. Lett.* 430, 523–532.
- Sun, S.S., McDonough, W.F., 1989. Chemical and isotopic systematics of oceanic basalts: Implications for mantle composition and processes. In: Saunders, A.D., Nory, M.J. (Eds.), *Magmatism in Ocean Basins*. Geological Society of London Special Publications 42, pp. 313–345.
- Teng, F.Z., Dauphas, N., Helz, R.T., 2008. Iron isotope fractionation during magmatic differentiation in Kilauea Iki Lava Lake. *Science* 320, 1620–1622.
- Teng, F.Z., Dauphas, N., Huang, S., Marty, B., 2013. Iron isotopic systematics of oceanic basalts. *Geochim. Cosmochim. Acta* 107, 12–26.
- Viti, C., Mellini, M., 1998. Mesh textures and bastites in the Elba retrograde serpentinites. *Eur. J. Mineral.* 10, 1341–1359.
- von Raumer, J., Stampfli, G.M., Arenas, R., Martínez, S.S., 2015. Ediacaran to Cambrian oceanic rocks of the Gondwana margin and their tectonic interpretation. *Int. J. Earth Sci.* 104, 1107–1121.
- Weyer, S., Ionov, D.A., 2007. Partial melting and melt percolation in the mantle: the message from Fe isotopes. *Earth Planet. Sci. Lett.* 259, 119–133.
- Williams, H.M., Bizimis, M., 2014. Iron isotope tracing of mantle heterogeneity within the source regions of oceanic basalts. *Earth Planet. Sci. Lett.* 404, 396–407.
- Williams, H.M., Peslier, A.H., McCammon, C., Halliday, A.N., Levasseur, S., Teutsch, N., Burg, J.P., 2005. Systematic iron isotope variations in mantle rocks and minerals: the effects of partial melting and oxygen fugacity. *Earth Planet. Sci. Lett.* 235, 435–452.
- Williams, H.M., Nielsen, S.G., Renac, C., Griffin, W.L., O'Reilly, S.Y., McCammon, C.A., Pearson, N., Viljoen, F., Alt, J.C., Halliday, A.N., 2009. Fractionation of oxygen and iron isotopes by partial melting processes: implications for the interpretation of stable isotope signatures in mafic rocks. *Earth Planet. Sci. Lett.* 283, 156–166.
- Wood, S.A., Samson, I.M., 2006. The aqueous geochemistry of gallium, germanium, indium and scandium. *Ore Geol. Rev.* 28, 57–102.
- Zhang, L., Sun, W.D., Zhang, Z., An, Y., Liu, F., 2019. Iron isotopic composition of supra-subduction zone ophiolitic peridotite from northern Tibet. *Geochim. Cosmochim. Acta* 258, 274–289.
- Zhang, L., Sun, W.D., Zhang, Z.F., An, Y., Liu, F., 2020. Iron isotope behavior during melt–peridotite interaction in supra-subduction zone ophiolite from Northern Tibet. *J. Geophys. Res. Solid Earth* 125 (2) e2019JB018823.
- Zhao, X.M., Zhang, H.F., Zhu, X.K., Tang, S.H., Tang, Y.J., 2010. Iron isotope variations in spinel peridotite xenoliths from North China Craton: implications for mantle metasomatism. *Contrib. Mineral. Petrol.* 160, 1–14.
- Zhao, X., Zhang, Z., Huang, S., Liu, Y., Li, X., Zhang, H., 2017. Coupled extremely light Ca and Fe isotopes in peridotites. *Geochim. Cosmochim. Acta* 208, 368–380.